HEP'99 # 5_522
Submitted to Pa 5
Pl 5

DELPHI 99-111 CONF 298
15 June 1999

Measurement of the semileptonic b branching ratios in Z decays

Preliminary

DELPHI Collaboration

Paper submitted to the HEP'99 Conference
Tampere, Finland, July 15-21

Measurement of the semileptonic b branching ratios in Z decays

Preliminary

DELPHI Collaboration

P.Antilogus[1], **I. Bozovic** [2], **M. Calvi**[3], **E. Cortina**[4], **Ch. de la Vaissière**[5], **M.Feindt**[6] **V. Lara**[4], **F. Martínez-Vidal**[4], **M.Margoni**[7], **J. Salt**[4], **F.Simonetto**[7], **P.Ronchese**[7], **J.Yi**[8]

[1] Université Claude Bernard de Lyon, IPNL, IN2P3-CNRS.
[2] Institute of Nuclear Physics, N.C.S.R. Demokritos Nuclear, Athens
[3] Università di Milano-Bicocca and INFN Sezione di Milano
[4] IFIC, Centro Mixto Univ. of Valencia – CSIC, Departamento de Física Atómica, Nuclear y Molecular
[5] LPNHE, IN2P3-CNRS, Univ. Paris VI et VII
[6] Institut für Experimentelle Kernphysik, Universität Karlsruhe.
[7] Università di Padova and INFN Sezione di Padova
[8] Department of Physics and Astronomy, Iowa State University, Ames.

Abstract

The semileptonic branching ratios for primary and cascade b decays BR(b$\to\ell^-$), BR(b$\to$c$\to\ell^+$) and BR(b$\to\bar{\text{c}}\to\ell^-$) were measured in hadronic Z decays collected by the DELPHI experiment at LEP from 1992 to 1995.

The sample was enriched in b decays using the lifetime information and various techniques were used to separate leptons from direct or cascade b decays.

By fitting the momentum spectra of di-leptons in opposite jets, the average b mixing parameter $\bar{\chi}_b$ was also extracted.

1 Introduction

This paper presents the measurement of inclusive semileptonic branching ratios of b quarks in hadronic Z decays using data collected with the DELPHI detector at LEP from 1992 to 1995. Four different analysis have been performed, using different strategies and partially overlapping statistical data samples.

Events containing b hadrons were selected using lifetime information, electrons and muons were tagged and various techniques were used to determine the origin of the lepton. Direct and cascade branching ratios: BR(b$\to\ell^-$), BR(b$\to$c$\to\ell^+$) and BR(b$\to\bar{\text{c}}\to\ell^-$) were measured, and by fitting the momentum spectra of di-leptons in opposite jets, the average b mixing parameter $\bar{\chi}_b$ was also extracted.

The plan of the paper is the following: a description of the DELPHI detector is given in Section 2 . The selection of the hadronic events sample is described in Section 3 . A brief summary of the relevant performances of lepton identification algorithms is given in section 5 .

The results of the single and di-lepton analysis are presented in Section 6, the results of the single lepton and jet-charge analysis are presented in Section 7, the Multitag analysis is described in Section 8 and the inclusive B-reconstruction analysis is described in Section 9.

Finally in section 10 averages among the results of the four analyses are calculated.

2 The DELPHI detector

The DELPHI detector has been described in detail in ref. [1]. Only the components relevant in this analysis are mentioned here.

In the barrel region, the charged particles are measured by a set of cylindrical tracking detectors whose axes are parallel to the 1.2 T solenoidal magnetic field and to the beam direction. The time projection chamber (TPC) is the main tracking device. The TPC is a cylinder with a length of 3 m, an inner radius of 30 cm and an outer radius of 122 cm. Tracks are reconstructed using up to 16 space points in the region $39^\circ < \theta < 141^\circ$, where θ is the polar angle with respect to the beam direction. Tracks can be reconstructed using at least 4 space points down to 21° and 159°.

Additional precise $R\Phi$ measurements, in the plane perpendicular to the magnetic field, are provided at larger and smaller radii by the Outer and Inner detectors respectively. The Outer Detector (OD) has five layers of drift cells at radii between 198 and 206 cm and covers polar angles from 42° to 138°. The Inner Detector (ID) is a cylindrical drift chamber having inner radius of 12 cm and outer radius of 28 cm. It contains a jet chamber section providing 24 $R\Phi$ coordinates surrounded by five layers of proportional chambers providing both $R\Phi$ and longitudinal z coordinates.

The micro-vertex detector (VD) is located between the LEP beam pipe and the ID [2]. It consists of three concentric layers of silicon microstrip detectors placed at radii of 6.3, 9.0 and 10.9 cm from the interaction region, called respectively: closer, inner and outer layer. For all layers the microstrip detectors provide hits in the $R\Phi$-plane with a measured intrinsic resolution of about 8 μm; the inner and outer layers provide in addition measurements in the z direction, with a precision depending on the polar angle

and reaching a value of 9 μm for tracks perpendicular to the modules. The polar angle coverage for charged particles hitting all three layers of the detector is $44^\circ < \theta < 136^\circ$; the closer layer coverage goes down to 25°. The z measurement was only available in 1994 and 1995.

The barrel electromagnetic calorimeter, HPC, covers the polar angles between 42° and 138°. It is a gas-sampling device which provides complete three dimensional charge information in the same way as a time projection chamber. Each shower is sampled nine times in its longitudinal development. Along the drift direction, parallel to the DELPHI magnetic field, the shower is sampled every 3.5 mm ; in the plane perpendicular to the drift the charge is collected by cathode pads of variable size, ranging from 2.3 cm in the inner part of the detector to 7 cm in the outer layers.

In the forward regions the tracking is completed by two sets of planar drift chambers (FCA and FCB) placed at distances of $\pm$165 cm and $\pm$275 cm from the interaction point. A lead glass calorimeter (EMF) is used to reconstruct electromagnetic energy in the forward region.

Muon identification in the barrel region is based on a set of muon chambers (MUB), covering polar angles between 53° and 127°. It consists of six active planes of drift chambers, two inside the return yoke of the magnet after 90 cm of iron (inner layer) and four outside after a further 20 cm of iron (outer and peripheral layers). The inner and outer modules have similar azimuthal coverage. The gaps in azimuth between adjacent modules are covered by the peripheral modules. Therefore a muon traverses typically either two inner layer chambers and two outer layer chambers, or just two peripheral layer chambers. Each chamber measures the $R\Phi$ coordinate with a precision of about 2-3 mm. Measuring $R\Phi$ in both the inner layer and the outer or peripheral layer determines the azimuthal angle of muon candidates leaving the return yoke within about $\pm 1^\circ$. These errors are much smaller than the effects of multiple scattering on muons traversing the iron.

In the forward region the muon identification is done using two sets of planar drift chambers (MUF) covering the angular region between 11° and 45°. The first set is placed behind 85 cm of iron and the second one behind an additional 20 cm. Each set consists of two orthogonal layers of drift chambers where the anode is read out directly and the cathode via a delay line to measure the coordinate along the wire. The resolution in both coordinates is about 4 mm.

3 Event selection

The decays of the Z to hadrons were selected by requiring:

- a total energy of the charged particles larger than 15 % of the centre-of-mass energy;
- at least 7 reconstructed charged particles.

  Charged particles were accepted if their polar angle was between 20° and 160°, their track length was larger than 30 cm, their impact parameter relative to the interaction point was less than 5 cm in the plane perpendicular to the beam direction and less

than 10 cm along the beam direction and their momentum was larger than 200 MeV/c with a relative error smaller than 100%.

Neutral particles detected in the HPC and EMF or in the hadronic calorimeters were required to have a measured energy larger than 500 MeV.

With these criteria, the efficiency to select $q\bar{q}$ events from the simulation was about 95%. All sources of background have been found to be below 0.1%. No significant differences in the acceptance between different flavours have been found.

For each event the thrust axis was calculated from all the charged and neutral particles selected as above. Only events with: $|\cos\theta_{thrust}| < 0.90$ were used.

Requiring, in addition, that all subdetectors needed for these analysis were fully operating, a total of about 1030000 and 515000 Z hadronic decays were selected from the 1994 and 1995 data sample respectively. About 3800000 events were selected from a simulated sample of $Z \to q\bar{q}$ events. A reduced angular region was used in some parts of the following analysis to assure a good vertex detector acceptance.

Events were generated with the JETSET 7.4 event generator [3] using parton shower and string fragmentation with parameters optimized to describe the hadronic distributions as measured by DELPHI. The events thus generated were passed through a detailed simulation [1] which modeled the detector response and processed through the same analysis chain as the real data .

Jets were formed from the charged and neutral particles using the JADE algorithm with $Y_{cut}^{min} = 0.02$ [4].

The transverse momentum of the lepton (p_t) was determined relative to the direction of the jet, excluding the lepton itself.

Any difference with these selection criteria, as well as their effect on the statistics used, will be explicitly described for each analysis.

4 b-flavour tagging

A b-flavour tagging algorithm was used in order to obtain a sample enriched in $Z \to b\bar{b}$ events. Analysis I,II and IV used the combined b-flavour tagging algorithm described in [5]. This algorithm combines in a single variable several quantities which are sensitive to the presence of a b-hadron. The main discriminant variable is the probability from all tracks belonging to the hemisphere to come from the primary vertex, calculated from the positively signed impact parameters of the tracks. Other variables were defined for hemispheres containing a secondary vertex. These variables are: the effective mass of particles used for the secondary vertex, the rapidity of tracks included in the secondary vertex with respect to the jet direction and the fraction of the charged energy of a jet included in the secondary vertex. Optimized levels of efficiency and purity were chosen in each analysis.

Analysis III used as a flavour tag a multivariate method, as described in section 8.1.1.

5 Lepton sample

5.1 Muon identification

To identify a charged particle with momentum greater than 3 GeV/c as a muon candidate, its track was extrapolated to each of the layers of the muon chambers taking into account multiple scattering in the material and the propagation of track reconstruction errors [6]. A fit was then made between the track extrapolation and the position and direction of the hits in the muon chambers. Ambiguities with muon chamber hits associated to more than one extrapolated track were resolved by selecting the track with the best fit. The charged particle was then identified as a muon if the fit was sufficiently good and hits were found outside the return iron yoke.

To exclude regions with poor geometrical acceptance, a muon was accepted if its polar angle, θ_μ, was within one of the following intervals:

$$0.03 < |\cos\theta_\mu| < 0.62$$
$$0.68 < |\cos\theta_\mu| < 0.95,$$

which defined the barrel and the forward regions, respectively.

The muon identification efficiency was measured in $Z \to \mu^+\mu^-$ events, in the decays of taus into muons and in muons from two-photons collisions $\gamma\gamma \to \mu^+\mu^-$. A mean efficiency of 0.82 ± 0.01 was found with little dependence on the muon momentum and the track polar angle. Predictions of simulation agree with data, both in absolute value and in the momentum dependence, within a precision of 2.0% and 2.5% in the barrel and in the forward region respectively. An estimate of the misidentification probability was obtained by mean of a lifetime-based anti b-tag, to select a background enriched sample. After the subtraction of the muon content in the selected sample the misidentification probability was found to be $(0.52 \pm 0.03)\%$ in the barrel and $(0.36 \pm 0.06)\%$ in the forward region. The ratio with the same quantity in simulated events was found to be in average 2.03 ± 0.12 (2.02 ± 0.13) in the barrel and 1.22 ± 0.20 (1.78 ± 0.24) in the forward region in the 1994 (1995) samples respectively, showing a little momentum dependence and a $\sim 30\%$ reduction near the border of the muon chambers geometrical acceptance.

The hadron misidentification probability, both in data and in simulation, was cross-checked using pions from K^0_s and τ decays and compatible results were found. In Analysis I, II and IV the simulated hadrons misidentified as muons were reweighted according to the probability measured in data. In Analysis III a different approach was used to estimate the misidentification probability, as described in section 8.2, and good agreement with the above results was found.

5.2 Electron identification

Charged particles with momenta greater than 3 GeV/c and within the efficient acceptance region of the HPC ($0.03 < |\cos\theta_e| < 0.72$) were accepted as electron candidates on the basis of the information from the HPC, the TPC and the Ring Imaging CHerenkov detector. Tracks were extrapolated to the HPC where showers were associated to them; signals from the various detectors have then been analyzed by a neural network [7].

The network response was analyzed in a sample of simulated electrons from b and c decays, and a momentum dependent cut was defined in order to have a 65% efficiency constant over the full momentum range.

The efficiency of tagging an electron was measured in the data by means of a set of isolated electrons extracted from selected Compton events and a set of electrons produced from photon conversions in the detector. The efficiency was then compared to that of the simulated event samples. The ratio of the experimental efficiency to the simulated one was parameterized in terms of the p_t and the polar angle of the track and found to be in average 0.92 ± 0.02 and 0.93 ± 0.02, in the 1994 and 1995 samples respectively. It was then applied to the sample of electrons in the simulated $q\overline{q}$ events.

The probability of tagging a hadron as an electron was measured in the data by selecting a background sample by means of an anti b-tag technique in the same manner as for muons. The measured misidentification probability in data, and the ratio with the same quantity in simulated events were in average $(0.40 \pm 0.02)\%$ and 0.76 ± 0.05 in the 1994 sample, $(0.38 \pm 0.04)\%$ and 0.70 ± 0.06 in the 1995 samples, respectively, showing a few percent relative increase at the HPC boundary.

To reduce the contamination from electrons produced from photon conversions, electron candidates were removed if they were consistent with coming from a secondary vertex and carrying no transverse momentum relative to the direction from the primary to the secondary vertex.

5.3 Simulated lepton sample

Samples of simulated events, which were processed through the same analysis chain as the data as described in Section 3, were used to obtain reference spectra for the different sources of simulated leptons.

The b semileptonic decays to electrons and muons were simulated using the IGSW model. The model of Bauer et al. [8], which takes into account the finite mass of the produced lepton, was used for the B decays into τ's. For D decays the branching ratios were adjusted to be better in agreement with measured values [9], and fulfilling isospin invariance. The different semileptonic decay modes, the branching ratios for the decays to neutral pions, when not measured, were obtained imposing isospin invariance. Reference spectra with alternative models have been obtained reweighting the events according to the decay model considered. The weight was computed on the basis of the lepton momentum in the B(D) rest frame. For the central value of the results, the ACCMM model was used, for the evaluation of the systematic error, the IGSW and ISGW** models were used, according to [10].

Leptons from the decay chain $b \to W \to \bar{c}q \to \ell^- X$ (the so called "upper vertex") were considered with both the contribution of $D_s \to \ell^- X$ and $\bar{D}^0(D^-) \to \ell^- X$.

6 Analysis I: Measurement of semileptonic b decays from single leptons and di-leptons spectra

In this analysis the semileptonic branching ratios for primary and cascade b decays BR(b$\to\ell^-$), BR(b$\to$c$\to\ell^+$) , BR(b$\to\bar{\rm c}\to\ell^-$) and the average b mixing parameter, $\bar{\chi}_b$, are measured using momentum spectra of single lepton and di-leptons in opposite jets. The single lepton spectra are studied in a sample of pure $b\bar{b}$ events, selected by means of a b-flavour tagging algorithm. For the di-lepton sample, an enriched $b\bar{b}$ purity is obtained by requiring a minimum p_t for one of the two leptons.

The sensitivity to the different sources of leptons is given by the kinematical properties of leptons from different sources and by the charge correlation between di-leptons in opposite jets from b and $\bar{\rm b}$ respectively.

With respect to a previous analysis [11] where a global fit to several electroweak parameters was performed, there is little dependence on the partial decay widths of the Z into $b\bar{b}$ and $c\bar{c}$ quark pairs ($R_b = \Gamma_{b\bar{b}}/\Gamma_{had}$, $R_c = \Gamma_{c\bar{c}}/\Gamma_{had}$) and the background due to misidentified hadrons and leptons from decays and punch-through of light hadrons is reduced.

Hadronic events and lepton candidates were selected as described in Sections 3 and 5. The angular region $|\cos\theta_{thrust}| < 0.9$ is used for di-lepton candidates, while for single lepton events, to have a good efficiency in the b-flavour tagging, events were considerd only if they verified $|\cos\theta_{thrust}| < 0.7$. As a consequence, only barrel muon chambers were considered for single muons. About 768000 and 385000 Z hadronic decays were selected in the 1994 and 1995 data samples, respectively.

6.1 Single lepton fit

Events were divided into two hemispheres, with respect to a plane perpendicular to the thrust axis and passing through the beam interaction point, and the primary vertex was reconstructed in each hemisphere. The combined b-flavour tagging algorithm described in section 4 was used to select hemispheres enriched in b-hadron content, while in the opposite hemisphere the single lepton spectra were studied. For the cut on the combined variable used in this analysis, the following efficiencies for selecting different flavours were estimated from simulation:

$\varepsilon_b = (39.34 \pm 0.05)\%$

$\varepsilon_c = (1.87 \pm 0.02)\%$

$\varepsilon_{uds} = (0.189 \pm 0.003)$ %

so that the fraction of b events in the sample was $\mathcal{P}_b = 95.1\%$.

The value of ε_b is quoted only for reference, since it is never used in the following. In practice the number N_b^H of tagged hemispheres which contain a b quark was estimated as:

$N_b^H = N_{tag}^H - (\varepsilon_c \times R_c + \varepsilon_{uds} \times R_{uds}) \times 2N_{had}$

where: N_{tag}^H and N_{had} are the total numbers of tagged hemispheres and the number of hadronic events, respectively, and $R_{uds} = \Gamma_{uds}/\Gamma_{had} = 1 - R_b - R_c$. For R_b and R_c the LEP average 0.2170 ± 0.0009 and 0.1734 ± 0.0048 were used respectively [12].

In the simulation, the same values N_b^H, ε_c and ε_{uds} were used.

Once an hemisphere was tagged as b, leptons were studied in the opposite one. A correction was applied, due to the correlation between the lifetime tag and the lepton tag. According to the simulation, it arised mainly from the acceptance requirements, which are different for electrons and muons, and amounted to $\rho_e = 1.003 \pm 0.005$ and $\rho_\mu = 1.017 \pm 0.005$. Here ρ is the ratio between the fraction of leptons tagged in a hemisphere opposite to a b-flavour tagged one and the fraction of leptons tagged in an unbiased b hemisphere. Before calculating the lepton transverse momentum, a search for secondary vertices was performed with the same algorithm as in [5]. If a secondary vertex was present in the jet, the jet direction was corrected using the primary to secondary vertex direction.

A binned maximum likelihood fit was used to compare the momentum and transverse momentum spectra of electrons and muons in data with the simulation.

Lepton candidates were classified according to their different origin as follows:

a) direct b-decay:
$\mathrm{b} \to \ell^- + \mathrm{X}$,

b) "right sign" cascade decays:
$\mathrm{b} \to \bar{\mathrm{c}} + \mathrm{X} \to \ell^- + \mathrm{X}$,

c) "wrong sign" cascade decays:
$\mathrm{b} \to \mathrm{c} + \mathrm{X} \to \ell^+ + \mathrm{X}$,

d) direct c-decay
$\mathrm{c} \to \ell^+ + \mathrm{X}$,

e) prompt leptons from J/Ψ decays or from b or c decays, where the $\mathrm{c\bar{c}}$ ($\mathrm{b\bar{b}}$) pair is produced by gluon splitting,

f) misidentified or decaying hadrons.

The above classification was considered both for electrons and muons, separately.

6.2 Di-lepton fit

The single lepton likelihood was multiplied by a likelihood obtained for di-leptons in opposite hemispheres, in order to separate the BR($\mathrm{b}\to\ell^-$) from the BR($\mathrm{b}\to\mathrm{c}\to\ell^+$) and the BR($\mathrm{b}\to\bar{\mathrm{c}}\to\ell^-$) components and to extract the average mixing parameter $\bar{\chi}_b$. In the di-lepton sample no b-flavour tag was used, in order not to introduce any bias in the composition of the b-hadrons sample. The b enrichment was obtained by requiring a minimum p_t for one of the two leptons. The full p_t spectra was considered for the opposite lepton. For a cut at $p_t > 1.2\ GeV/c$, a b purity of about 88% was obtained using simulated events.

Di-lepton events were separated, for both the data and the simulated samples, into six categories depending on whether the two lepton candidates have the same or opposite charge and on which combination of lepton species (ee, $e\mu$, $\mu\mu$) they belonged to. Lepton pairs were used if the two leptons were separated by at least 90^o, while lepton

pairs coming from the same jet were omitted from the fit to avoid additional systematic uncertainties in the composition of the cascade lepton sample. For each category, simulated events were separated into the above mentioned classes (a-f). To guarantee a reasonable number of events in each bin, the p and p_t of each lepton in the pair were combined to form one variable, the combined momentum, p_c, defined as $p_c = \sqrt{p_t^2 + \frac{p^2}{100}}$. Two-dimensional reference distributions were obtained for the chosen combinations in the variables (p_c^{min}, p_c^{max}), where p_c^{min} (p_c^{max}) refers to the smallest (largest) combined momentum.

If $B^0 - \bar{B}^0$ mixing is not considered, the main source of di-leptons having opposite charges are direct b-decays: $(\mathrm{b} \to \ell^-)(\bar{\mathrm{b}} \to \ell^+)$. But, in the presence of mixing, a fraction $2\bar{\chi}_b(1 - \bar{\chi}_b)$ of these di-leptons have the same charge. Same charge di-leptons also arise from events with one direct b-decay and one cascade b-decay: $(\mathrm{b} \to \ell^-)(\bar{\mathrm{b}} \to \bar{\mathrm{c}} \to \ell^-)$. Because of mixing a fraction $2\bar{\chi}_b(1 - \bar{\chi}_b)$ of these events will enter the opposite charge class.

6.3 Results and systematic errors

The results obtained with the 1994 and 1995 samples and their combination are shown in table 1, where the errors are statistical only.

	1994	1995	1994+1995
$\mathrm{BR}(\mathrm{b}\to\ell^-)$	0.1064 ± 0.0013	0.1069 ± 0.0018	0.1066 ± 0.0011
$\mathrm{BR}(\mathrm{b}\to\mathrm{c}\to\ell^+)$	0.0824 ± 0.0047	0.0781 ± 0.0062	0.0808 ± 0.0037
$\mathrm{BR}(\mathrm{b}\to\bar{\mathrm{c}}\to\ell^-)$	0.0145 ± 0.0042	0.0206 ± 0.0053	0.0168 ± 0.0033
$\bar{\chi}_b$	0.119 ± 0.016	0.138 ± 0.022	0.1256 ± 0.013

Table 1: Results of the fit to the 1994 and 1995 lepton samples and their combination. The errors are statistical only.

The Peterson fragmentation parameter [13], ϵ_b, was left free to vary in the fit. Converted into the mean fractional energy of b-flavoured hadrons it gives $\langle x_E \rangle = 0.7126 \pm 0.0031$, where the error is statistical only.

In figure 1 single lepton and di-lepton spectra are shown. The simulation spectra have been reweighted according to the result of the fit.

The correlation matrix for the statistical error is shown in table 2.

	$\mathrm{BR}(\mathrm{b}\to\ell^-)$	$\mathrm{BR}(\mathrm{b}\to\mathrm{c}\to\ell^+)$	$\mathrm{BR}(\mathrm{b}\to\bar{\mathrm{c}}\to\ell^-)$	$\bar{\chi}_b$	ϵ_b
$\mathrm{BR}(\mathrm{b}\to\ell^-)$	1.00	-0.246	-0.067	0.087	0.202
$\mathrm{BR}(\mathrm{b}\to\mathrm{c}\to\ell^+)$		1.00	-0.795	-0.157	-0.050
$\mathrm{BR}(\mathrm{b}\to\bar{\mathrm{c}}\to\ell^-)$			1.00	0.109	-0.036
$\bar{\chi}_b$				1.00	0.018
ϵ_b					1.00

Table 2: Correlation matrix of statistical uncertainties.

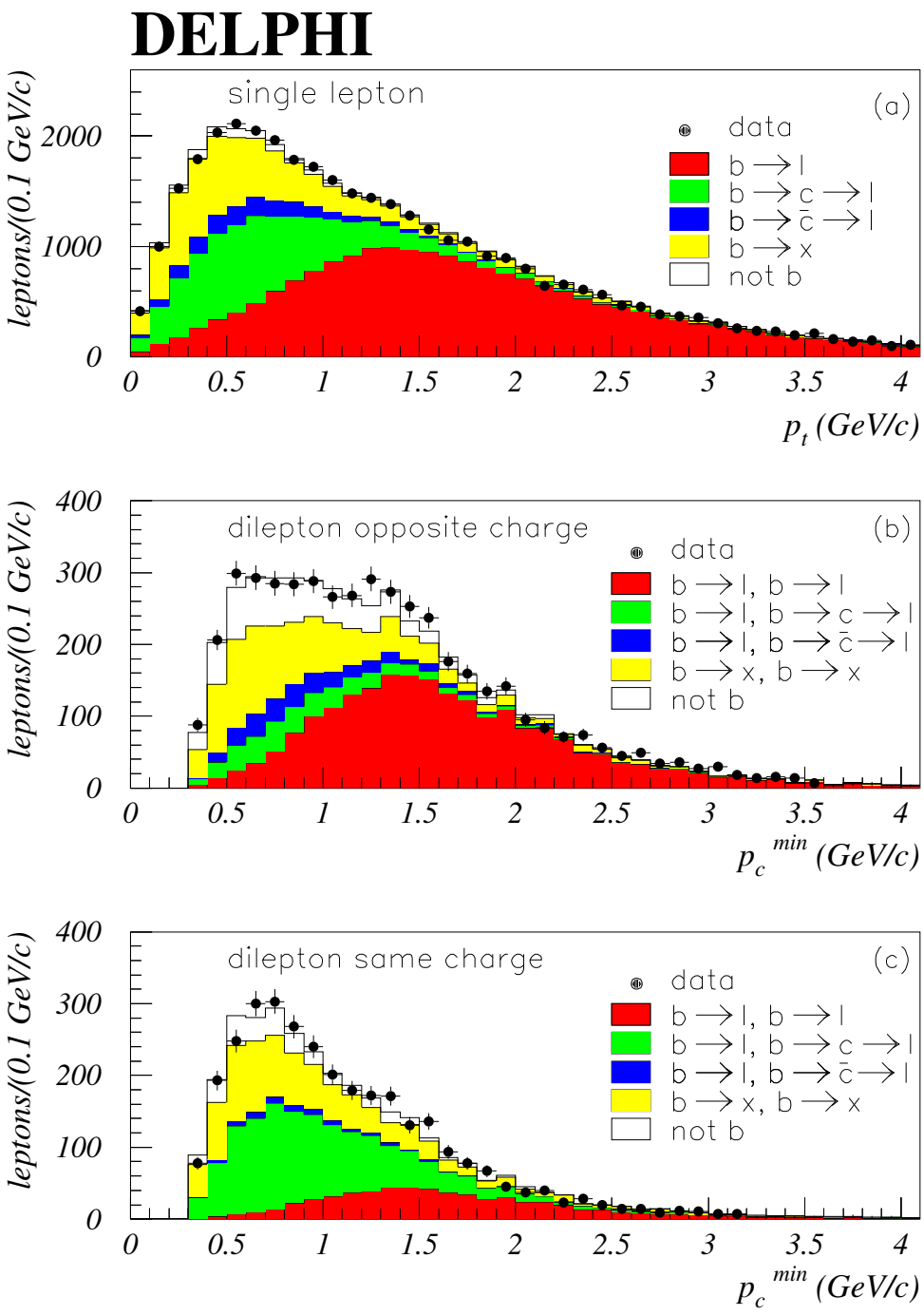

Figure 1: Comparison of data and simulation spectra. The simulation spectra have been reweighted according to the result of the fit. (a) Transverse momentum distribution for single electrons and muons. (b) Combined momentum distribution for the two leptons in di-lepton events, identified in opposite jets and having an opposite charge. (c) Combined momentum distribution for the two leptons in di-lepton events, identified in opposite jets and having the same charge. In (b) and (c) the p_c^{min} refers to the minimum combined momentum of the two leptons.

Error Source	Range	ΔBR(b$\to\ell^-$) 10^{-2}	ΔBR(b$\to$c$\to\ell^+$) 10^{-2}	ΔBR(b$\to\bar{\text{c}}\to\ell^-$) 10^{-2}	$\Delta\bar{\chi}_b$ 10^{-2}
electron efficiency	$\pm 3\%$	∓ 0.15	∓ 0.14	∓ 0.06	± 0.02
misidentified e	$\pm 8\%$	∓ 0.05	∓ 0.14	∓ 0.06	± 0.04
converted photons	$\pm 10\%$	<0.01	∓ 0.06	∓ 0.03	± 0.01
μ efficiency barrel	$\pm 2.8\%$	∓ 0.15	∓ 0.20	∓ 0.06	± 0.06
μ efficiency forward	$\pm 3.2\%$	∓ 0.03	∓ 0.01	∓ 0.01	∓ 0.02
misidentified μ bar.;for.	$\pm 6.5\%;17\%$	∓ 0.01	∓ 0.15	∓ 0.06	± 0.02
jet direction	0.8°	$+0.05$	-0.03	-0.08	+ 0.6
ε_c	$\pm 9\%$	± 0.02	∓ 0.01	∓ 0.01	± 0.03
ε_{uds}	$\pm 22\%$	± 0.01	± 0.02	∓ 0.0	∓ 0.02
$\ell - b$ correlation	$\pm 1\%$	∓ 0.05	∓ 0.11	∓ 0.03	± 0.03
R_b	0.2170 ± 0.0009	<0.01	<0.01	<0.01	<0.01
R_c	0.1734 ± 0.0048	± 0.01	± 0.01	± 0.01	∓ 0.01
$\langle x_E(\text{c})\rangle$	0.484 ± 0.008	∓ 0.02	± 0.03	∓ 0.03	± 0.02
$\frac{b\to W\to D}{b\to W\to D_s}$	$(1.28^{+1.52}_{-0.61})$	± 0.03	$^{+0.20}_{-0.11}$	$^{-0.23}_{+0.13}$	$^{-0.09}_{+0.07}$
Br(b $\to \tau \to \ell$)	$(0.452 \pm 0.074)\%$	∓ 0.02	∓ 0.03	∓ 0.04	± 0.02
Br(b $\to$ J/$\psi \to \ell^+\ell^-$)	$(0.07 \pm 0.02)\%$	∓ 0.05	± 0.01	± 0.01	∓ 0.18
Br(c $\to \ell$)	$(9.8 \pm 0.5)\%$	∓ 0.02	∓ 0.04	∓ 0.07	± 0.01
g $\to$ c$\bar{\text{c}}$	$(2.33 \pm 0.50)\%$	<0.01	<0.01	<0.01	<0.01
g $\to$ b$\bar{\text{b}}$	$(0.269 \pm 0.067)\%$	<0.01	<0.01	<0.01	± 0.01
total systematic		± 0.24	± 0.38	± 0.25	± 0.69
Semilept.mod.b $\to \ell$[10]	ACCMM ($^{+\text{ISGW}}_{-\text{ISGW}**}$)	$^{-0.24}_{+0.41}$	$^{+0.23}_{-0.29}$	$^{+0.14}_{-0.23}$	$^{-0.23}_{+0.28}$
Semilept.mod.c $\to \ell$[10]	ACCMM1($^{+\text{ACCMM2}}_{-\text{ACCMM3}}$)	$^{-0.08}_{+0.07}$	$^{-0.11}_{+0.01}$	$^{-0.03}_{+0.02}$	$^{-0.33}_{+0.34}$
total models		$^{-0.25}_{+0.42}$	$^{-0.31}_{+0.23}$	$^{-0.23}_{+0.14}$	$^{-0.40}_{+0.44}$

Table 3: Summary of systematic uncertainties in the analysis of single and di-lepton events. The range is given in %, it corresponds to a relative variation around the central value.

The following sources of systematic uncertainty have been considered:

- experimental uncertainty related to lepton measurements:

  the muon and electron identification efficiencies and the background due to hadron misidentification have been varied considering their measurement errors in the data-simulation comparisons (see sections 5.1,5.2). To account for effects related to the difference in topology between the test samples used in sections 5.1,5.2 and the hadronic environment, an additional uncertainty of $\pm$ 2% has been considered on the efficiencies, as estimated from simulation.

  The residual contamination in the electron sample due to converted photons has been varied by $\pm$ 10%.

  The systematic error due to the uncertainty on the b-quark direction and consequently on the lepton transverse momentum has been evaluated comparing the jet momentum direction with the direction determined by the secondary vertex in case it was successfully reconstructed. The mean difference in the jet direction was found to be 1.5°; the fit has then been performed using both methods and half difference on the results has been used as systematic error.

- experimental uncertainty related to the b-flavour tagging:

  efficiencies to tag c and uds quarks have been varied according to the errors in [5]. The correlation between the lifetime tag and the lepton tag has been varied to twice its statistical error. The partial decay widths R_b and R_c have been varied according to their measurement errors.

  The stability of the result as a function of the cut on the b-flavour tagging variable has been checked to be compatible with the corresponding statistical fluctuations.

- the modelling uncertainty related to the assumed branching ratios and to different lepton decay models has been calculated according to [10].

The summary of systematic uncertainties is given in table 3.

In conclusion from a fit to single and di-lepton events from data collected with the DELPHI detector in 1994 and 1995, the semileptonic branching ratios BR(b$\to\ell^-$), BR(b$\to$c$\to\ell^+$), BR(b$\to\bar{\text{c}}\to\ell^-$) and the average b mixing parameter $\bar{\chi}_b$ have been measured:

$$
\begin{aligned}
\text{BR}(\text{b}\to\ell^-) &= (10.66 \pm 0.11(stat) \pm 0.24(syst)^{-0.25}_{+0.42}(model))\% \\
\text{BR}(\text{b}\to\text{c}\to\ell^+) &= (8.08 \pm 0.37(stat) \pm 0.38(syst)^{-0.31}_{+0.23}(model))\% \\
\text{BR}(\text{b}\to\bar{\text{c}}\to\ell^-) &= (1.68 \pm 0.33(stat) \pm 0.25(syst)^{-0.23}_{+0.14}(model))\% \\
\bar{\chi}_b &= 0.1256 \pm 0.013(stat) \pm 0.007(syst) \pm 0.004(model)
\end{aligned}
$$

7 Analysis II: Measurement of semileptonic b decays from single leptons and jet-charge

A sample of b enriched events was obtained by applying b-flavour tagging separately to each hemisphere of the event: therefore only the events with thrust axis contained in the barrel region ($|\cos(\theta_{thrust})|<0.8$) were used. The b tagging algorithm exploited only the information from the impact parameters of the tracks from charged particles assigned to the hemisphere: the cut selected 69.2 % $b\bar{b}$, 12.9 % $c\bar{c}$ and 1.1 % uds events, so that the fraction of b events in the sample was $\mathcal{P}_b = 84.0\%$. Leptons were then selected from all the charged particles with momentum $p > 2$ GeV/c, lying in the hemisphere opposite to the b-tagged one within the acceptance of the HPC or of the muon chambers. As compared to the other analyses, tighter lepton identification cuts were applied.
The lepton was then used as a seed to reconstruct the position of the B decay vertex, by applying the algorhitm originally developed for lifetime and oscillation measurements (for details, see e.g. [14]). A vertex was found in 92.5 (92.3) % of the cases in the data (simulation). The direction of the b-hadron was then obtained by averaging the direction of the jet containing the lepton with the one of the vector joining the primary to the secondary vertex: when the vertex was not reconstructed, only the jet direction was used. The energy of the b hadron was computed from the sum of the energy of the charged and neutral particles assigned to its jet and the missing energy in the hemisphere (computed as described in [15]). The resolution was $\sigma(E_B)/E_B \simeq 12\%$. This allowed to reconstruct entirely the b-hadron four momentum, by assuming an average mass of $\simeq 5.3$ GeV/c^2.
Leptons from direct $b\to\ell^-$decays were then separated from the background ($b\to c\to\ell^+$, $c\to\ell^+$, fake hadrons, etc.) by means of

- kinematics: the momentum of the lepton in the b-hadron rest frame, k^* , was computed by boosting back the lepton in the b rest frame: the resolution was about $\sigma_{k^*} \simeq 200\ MeV/c$. The k^* spectra for $b\to\ell^-$,$b\to c\to\ell^+$,$c\to\ell^+$ decays in the simulation were tuned as described in chapter 5.3 and varied according to the prescriptions already described to compute the systematic error;

- charge correlation: the electric charge of the lepton was compared to the one of the b hadron in the other hemisphere. Neglecting mixing, the product $\lambda_Q = Q_\ell \cdot Q_b$ should be -1/3 (+1/3) for leptons from direct (cascade) decays. The charge of the b quark was however determined in each hemisphere by properly combining several quantites (jet charge, vertex charge, charge of any kaon or lepton from b decay, charge of leading fragmentation particles: a detailed description of the method can be found in [16]), so that λ_Q actually ranged between -1 (mostly $b\to\ell^-$) and +1 (mostly $b\to c\to\ell^+$). Figure 2 shows the λ_Q distribution for the data (crosses) and simulation (upper histogram). The fraction of wrong charge assignment, for a given λ_Q range, depends on several quantities related both to the B hadron production and decay mechanism (B mixing, fragmentation, lepton and K production in B decays, B charged multiplicity, etc.) and to the detector performance (tracking, vertexing, particle id.), which are in some cases not well known. To reduce the systematic uncertainty, the fraction of correct tags (η_{λ_Q}) was determined in the data,

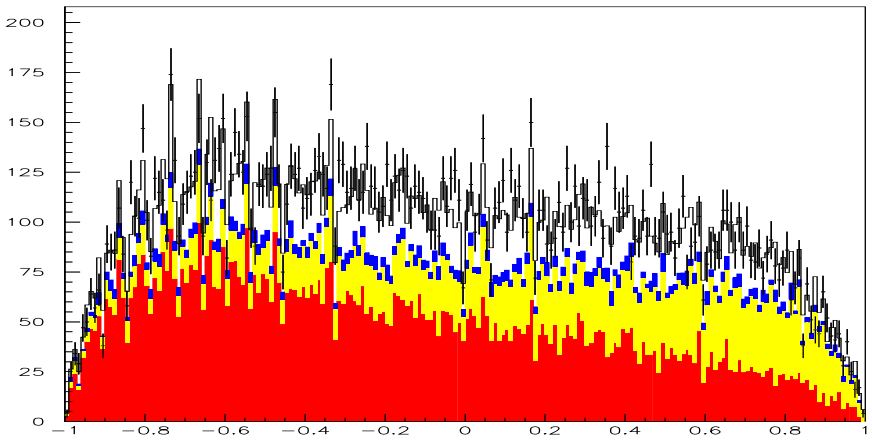

Figure 2: λ_Q distrution for data (crosses) and simulation (upper histogram). The contributions from $b\to\ell^-$ events is given by the dark grey area, the $b\to c\to\ell^+$ ($b\to\bar{c}\to\ell^-$) contribution is represented by the light (darker) grey area.

as explained below. Contrary to the previous analysis, where the charge correlation could be exploited only in case of double semileptonic decays, the variable λ_Q could be determined for all the events: it should be noted however that the discrimination power of this variable is smaller. Therefore the two analyses are complementary. Only 1994 data were used for this analysis.

7.1 Determination of the branching fractions

The b semileptonic branching fractions were obtained by means of a binned χ^2 fit. Leptons in the data and in the simulation were collected in two-dimensional bins, according to their k^* and λ_Q values, so as to exploit at best the discriminating power of the two variables. The k^* bins had variable size, determined to have at least twenty entries in each bin. The λ_Q space was divided in an even number (N_{λ_Q}) of equally spaced bins.

Events in the simulation were assigned to one of the six categories described in section 6.1 depending on their origin. Leptons from categories (c) to (f) were normalised to the data according to the number of hadronic events, known branching ratios and efficiency correction factors. The normalisation factors for the categories (a) and (b) were instead determined from the fit and used to compute the branching ratios for the direct ($b\to\ell^-$) and cascade ($b\to c\to\ell^+$) semileptonic decays. In order to determine in addition the Br($b\to\bar{c}\to\ell^-$), the fit was then repeated letting also the normalisation of category (c) as a further free parameter. Figure 3 shows the fitted k^* distribution in four different λ_Q bins.

The fraction of correct charge tags in each λ_Q bin was determined while performing the

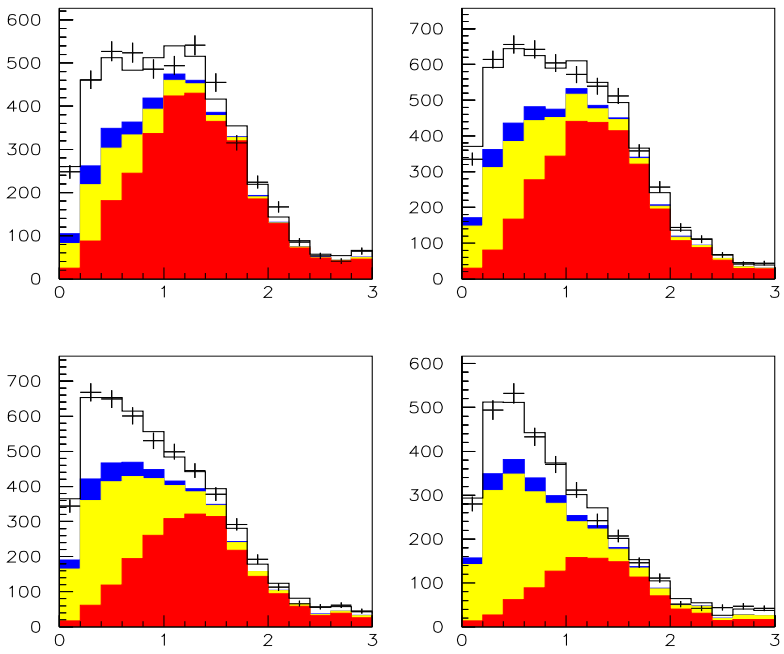

Figure 3: k^* distribution (in GeV/c) for the data (crosses) and the fitted simulation (upper histogram). The lower histograms represent the contributions from from $b \to \ell^-$ (dark grey) $b \to c \to \ell^+$ (light grey) and $b \to \bar{c} \to \ell^-$ (darker grey). The four plots are obtained by requiring, respectively: $-1 < \lambda_Q < -.5, -.5 < \lambda_Q < 0., 0. < \lambda_Q < .5, .5 < \lambda_Q < 1$.

fit. For this purpose, the total number of simulated events belonging to the category ℓ (ℓ=a,b,c) and falling in the i^{th} (j^{th}) k^* (λ_Q) bin where multiplied by a (linear) correction factor:

$$\mathcal{N}^\ell(i,j) \;=\; \mathcal{N}_0{}^\ell(i,j) \;\cdot\; (1+\delta_j^\ell)$$

The δ coefficients would be zero if the simulation described the data perfectly. They were left as free parameters in the fit with the following constraints:

- for a given λ_Q bin, δ does not depend on k^*
- $\delta_j^a = \delta_j^c = \delta_k^b$, where k is the complementary λ_Q bin to j ($k = N_{\lambda_Q} + 1 - j$);
- $\Sigma_i \mathcal{N}^\ell(i,j) \;=\; \Sigma_i \mathcal{N}_0^\ell(i,j) \;\forall\; \ell, j$

The first two requests follow from the fact that the λ_Q tag is performed in the opposite hemisphere, and is therefore uncorrelated to the k^* tag and any other lepton decay property; the third constraint ensures that the total number of events is conserved. The fit results did not change significantly if the same correction was applied to the simulated leptons of the other classes (d-f).
Due to the momentum cut, the efficiency to select a lepton depends on the boost transferred to the b-hadron during the fragmentation process. To reduce this model dependence, the energy spectra of the b-hadrons in the data and in the simulation where compared and the value of the Peterson fragmentation parameter ϵ_b [13] which best describes the data was determined. The measurement proceeded by iteration: first , the branching ratios were determined by assuming the ϵ_b value as in the simulation, then the lepton sample composition was recomputed according to those branching ratios and ϵ_b was fitted; the branching ratios were determined again assuming the new ϵ_b value, and so on until convergence, which was in fact reached after the first iteration. The fitted value $\epsilon_b \;=\; (0.2441 \pm 0.0035) \cdot 10^{-2}$ corresponds to a mean b-hadron energy $X_E \;=\; 0.7033 \pm 0.0004$ (stat.) ± 0.004 (syst.): the systematic error is dominated by the uncertainty on the mean energy of $\pm 200\ MeV$.
The procedure was performed separately for muons and electrons: consistent results were found. The χ^2 per degree of freedom was 1.08 for muons and 1.27 for electrons (see also Figure 3): there was no appreciable difference in the χ^2 when using different models to describe the lepton spectra. The final average values are:

$$\begin{aligned} Br(b\to\ell^-) &= (10.74 \pm 0.13(stat.) \pm 0.41(exp.syst.)^{+0.46}_{-0.30})(model)\% \\ Br(b\to c\to\ell^+) &= (\ 8.43 \pm 0.22(stat.) \pm 0.41(exp.syst.)^{+0.67}_{-0.78})(model)\% \end{aligned}$$

for the fit with two parameters and

$$\begin{aligned} Br(b\to\ell^-) &= (10.68 \pm 0.14(stat.) \pm 0.31(syst)^{+0.50}_{-0.32})(model)\% \\ Br(b\to c\to\ell^+) &= (\ 7.22 \pm 0.66(stat.) \pm 0.35(syst)^{+0.50}_{-0.34})(model)\% \\ Br(b\to \bar{c}\to\ell^-) &= (\ 2.00 \pm 0.45(stat.) \pm 0.38(syst)^{+0.55}_{-0.80})(model)\% \end{aligned}$$

for the other one. The breakdown of the systematic errors for the three parameter fit is presented in table 4.

Error Source	Range	ΔBR(b$\to\ell^-$) 10^{-2}	ΔBR(b$\to$c$\to\ell^+$) 10^{-2}	ΔBR(b$\to\bar{\text{c}}\to\ell^-$) 10^{-2}
electron efficiency	$\pm 3.\%$	∓ 0.17	∓ 0.16	∓ 0.13
electron background	$\pm 10.\%$	± 0.03	∓ 0.14	∓ 0.18
μ efficiency	$\pm 2.8\%$	∓ 0.20	∓ 0.15	∓ 0.08
μ background	$\pm 15.\%$	< 0.01	∓ 0.03	∓ 0.10
ε_c	$\pm 9\%$	± 0.13	∓ 0.09	± 0.02
ε_{uds}	$\pm 22\%$	± 0.03	± 0.02	<0.01
$\ell - b$ correlation	$\pm 1.\%$	∓ 0.05	∓ 0.11	∓ 0.03
R_b	0.2170 ± 0.0009	<0.01	<0.01	<0.01
R_c	0.1734 ± 0.0048	± 0.01	± 0.01	∓ 0.01
binning		$\pm$ 0.05	$\pm$ 0.05	$\pm$ 0.05
total experimental		± 0.30	± 0.30	± 0.26
$\langle x_E(\text{c})\rangle$	0.484 ± 0.008	∓ 0.02	± 0.02	-
$\frac{b\to W\to D}{b\to W\to D_s}$	$(1.28^{+1.52}_{-0.61})$	± 0.03	$^{+0.20}_{-0.11}$	$^{-0.23}_{+0.13}$
Br(b $\to \tau \to \ell$)	$(0.452 \pm 0.074)\%$	∓ 0.01	∓ 0.05	∓ 0.09
Br(b $\to$ J/$\psi \to \ell^+\ell^-$)	$(0.07 \pm 0.02)\%$	∓ 0.06	± 0.08	∓ 0.18
Br(c $\to \ell$)	$(9.8 \pm 0.5)\%$	∓ 0.03	< 0.01	± 0.02
g $\to$ c$\bar{\text{c}}$	$(2.33 \pm 0.50)\%$	<0.01	<0.01	<0.01
g $\to$ b$\bar{\text{b}}$	$(0.269 \pm 0.067)\%$	<0.01	<0.01	<0.01
total systematics		± 0.31	± 0.35	± 0.38
Semilept.mod.b $\to \ell$[10]	ACCMM $(^{+\text{ISGW}}_{-\text{ISGW}**})$	$^{-0.30}_{+0.50}$	$^{-0.30}_{+0.45}$	$^{-0.74}_{+0.50}$
Semilept.mod.c $\to \ell$[10]	ACCMM1$(^{+\text{ACCMM2}}_{-\text{ACCMM3}})$	$^{-0.08}_{+0.05}$	$^{-0.07}_{+0.02}$	$^{-0.05}_{+0.03}$
total models		$^{-0.31}_{+0.50}$	$^{-0.31}_{+0.45}$	$^{-0.74}_{+0.50}$

Table 4: Summary of systematic uncertainties in the analysis of lepton vs jet charge. If a range is given in % it means a relative variation around the central value.

8 Analysis III: Measurement of semileptonic b decays by applying a multitag method

A measurement of BR($b \to \mu$) and BR($b \to c(\bar{c}) \to \mu$) using data collected with the DELPHI detector between 1992 and 1995 is presented here.

In this analysis the contributions of uds, c and b flavours were separated in an inclusive way with a multitag method. This method used almost all the hadronic events, because it was based on a flavour deconvolution without the need for any further cuts. One important by-product of the method was a systematic and independent analysis of the muon background.

The selection of the hadronic events was almost the same as in section 3 with the only difference that 5 charged particles, instead of 7, were required to select the event, and that the event thrust axis was required to be within the barrel region: $|\cos\theta_{th}| < 0.75$.

The total number of selected events both in real and simulated data are:

	1992	1993	1994	1995	Total
Simulated	1369156	1232678	2275552	712868	5590254
Real data	486357	471437	971448	467809	2397051

Muons are identified as described in section 5.1.

8.1 Flavour tagging and flavour deconvolution

8.1.1 Flavour tagging

For flavour-tagging, the multivariate method described in reference [17] was used. This method tags the two event hemispheres, defined with the plane perpendicular to the thrust axis, and provides two important features: a) minimal correlation between hemispheres, in particular because the event vertex is computed independently in each hemisphere and b) direct measurement on data of tagging efficiencies and flavour compositions. These two properties are important. The former because an independent and uncorrelated tag of the hemisphere with muon identification is needed and the latter because the formalism of the analysis requires the knowledge of the efficiencies and flavour compositions.

The classification criteria is based on the so-called flavour multivariate discriminators which combine the multivariate and the confidence tags as described in reference [18]. The flavour tag is assigned by applying cuts in a priority order to the discriminators. Inside a tag, hemispheres are subdivided into categories with additional cut criteria, trying to have at least one category in each flavour with maximum efficiency and the lowest possible background. In this analysis a set of six categories have been used. Since 1994, due to the introduction of double sided vertex detectors, a better b-tagging has been achieved. Moreover, in this analysis a good tagging performance in the charm sector is important and the cuts defining the working point has been chosen in order to optimize the efficiency.

The split into two hemispheres allows a fit that provides the so called tagging parameters: R_j, fraction of flavour j hemispheres in the sample, and ε_I^j, probability to classify an hemisphere of flavour j in the category I. The parameters were obtained directly from data with a minimal reference to models. This method was succesfully applied to the $\Gamma_{b\bar{b}}/\Gamma_{had}$ determination ([5]).

8.1.2 Flavour deconvolution

The aim of the flavour deconvolution is to extract the spectra of the muon variables for each flavour. The inputs to this deconvolution are the distributions (not shown here) of a muonic observable for each category. Three different variables have been considered in this analysis: p, p_t^{in} and p_t^{out}, where p is the momentum of the muon candidate and p_t^{in} and p_t^{out} are the muon transverse momentum with respect to the jet axis including or excluding the muon in the definition of the jet. Hereafter any of these variables will be referred as z. Other variables can be chosen under the requirement that the b tagging does not depend on these variables.

The category assigned to an identified muon is the category found by the tagging in the opposite hemisphere. The aim of doing this is to avoid correlations between the hemisphere tagging and the presence of the muon.

The chosen observable is the number of identified muons in a given category, I, in an interval of z ($n_I^\mu(z)$). In the same interval, a χ^2 function can be defined as:

$$\chi^2 = \sum_I \frac{\left(n_I^\mu(z) - N_{hem}\left(\sum_j \varepsilon_I^j R_j D_j^\mu(z)\right)\right)^2}{\sigma^2\left(n_I^\mu(z)\right)} \tag{1}$$

where N_{hem} is the total number of hemispheres, R_j and ε_I^j are the tagging parameters and $D_j^\mu(z)$ is the muon variable spectrum for the flavour j in a given hemisphere. The above formula neglects correlations between hemisphere tagging and muon selection efficiencies in opposite hemispheres.

The minimization of this function leads to a set of three linear equations for each z bin where the three unknowns are the components of the spectrum in each flavor : $D_{uds}^\mu(z)$, $D_c^\mu(z)$, $D_b^\mu(z)$. These quantities, and their errors, are computed by solving these equations.

In order to check the validity of the method a test has been performed using simulated data. Figure 4 compares, in the case of $z = p_t^{out}$, the result of the deconvolution with the generated distribution.

The result of the deconvolution can be written as a function of the different sources of identified muons:

$$\begin{aligned} n_{uds}^\mu(z) =& N_{hem} R_{uds} D_{uds}^\mu(z) = n_{uds}^{f\mu}(z) \\ n_c^\mu(z) =& N_{hem} R_c D_c^\mu(z) = n_c^{p\mu}(z) + n_c^{f\mu}(z) \\ n_b^\mu(z) =& N_{hem} R_b D_b^\mu(z) = n_b^{p\mu}(z) + n_b^{c\mu}(z) + n_b^{f\mu}(z) \end{aligned} \tag{2}$$

where $n_{uds}^{f\mu}(z)$, $n_c^{f\mu}(z)$ and $n_b^{f\mu}(z)$ are the distributions of *fake* muons for different flavours, $n_b^{c\mu}(z)$ is the distribution of muons coming from c (including $c\bar{c}$) *cascade* secondary decays of the b and $n_c^{p\mu}(z)$ and $n_b^{p\mu}(z)$ are the distributions of *prompt* muons coming from c and b decays respectively. In the b flavour, the distribution $n_b^{g\mu}(z)$ of *genuine* muons can be expressed as $n_b^{g\mu}(z) = n_b^{p\mu}(z) + n_b^{c\mu}(z)$.

This method of flavour deconvolution can also be applied to other kind of particles and observables. For example, the deconvolution can be applied to all charged particles. The distributions obtained with charged particles are an interesting result by themselves. Here they are used to compute background as described in the next section.

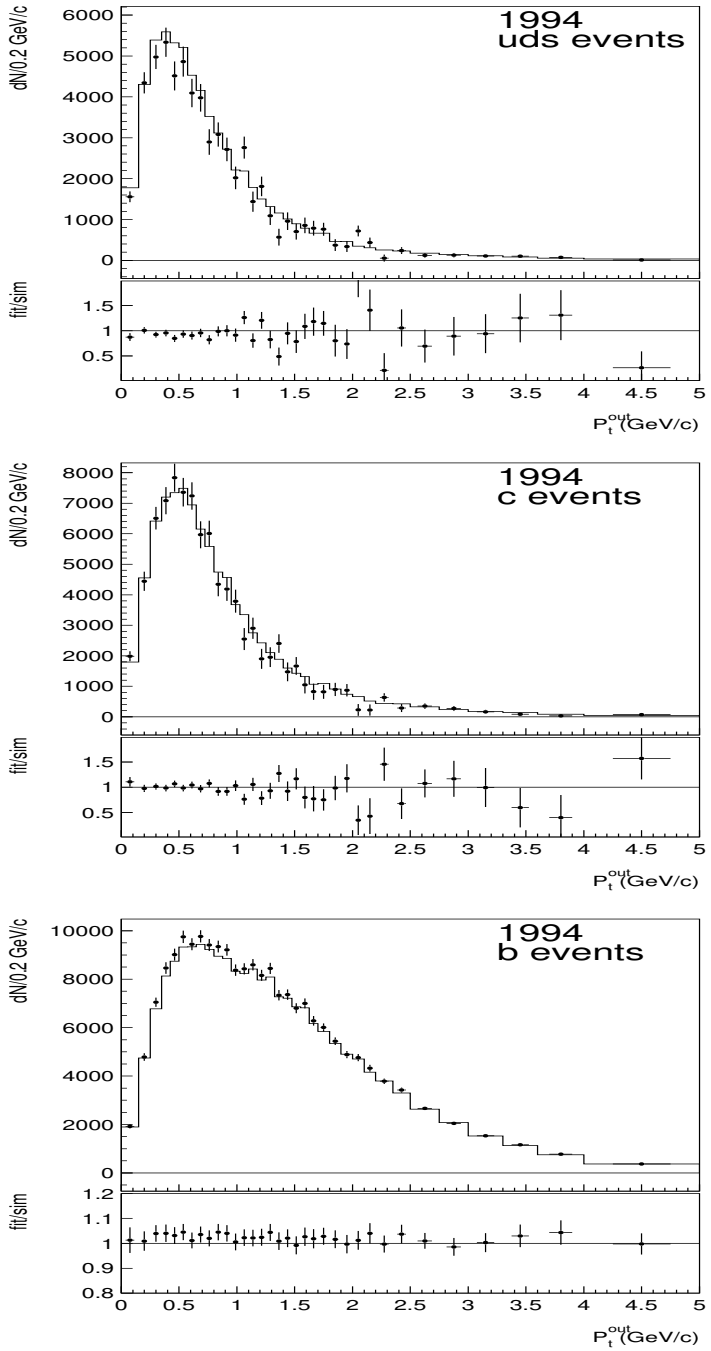

Figure 4: Separation of p_t^{out} spectra of candidate muons between the three flavors. In the upper plot is shown the comparison between generated (solid line) and the results of the deconvolution (points). In the lower plot is shown the ratio between these two distributions which exhibits a high agreement with 1.

8.2 Background extraction and hadron misidentification probability

In this analysis a fake muon is defined as any particle identified as muon that, either is not a muon, or is a muon but from a light hadron decay (mainly pion or kaon). Following this definition, all identified muons in uds events are fake, the fraction of heavy quark production from gluon splitting can be assumed to be negligible. Then a misidentification probability, η_{uds}, can be defined as the fraction of identified muons in uds events:

$$\eta_{uds}(z) = \frac{n^{\mu}_{uds}(z)}{n^{tk}_{uds}(z)} \tag{3}$$

where $n^{tk}_{uds}(z)$ is the spectrum of charged particles with the same kinematical cuts as the muons in the uds sector. In an accurate approach, the uds misidentification probability can be expressed as:

$$\eta_{uds}(z) = \eta^{\pi}(z)\bar{f}^{\pi}_{uds}(z) + \eta^{k}(z)\bar{f}^{k}_{uds}(z) + \eta^{\mu}(z)\bar{f}^{\mu}_{uds}(z) + \eta^{o}(z)\bar{f}^{o}_{uds}(z) \tag{4}$$

where $\eta^{\pi}(z)$ and $\eta^{k}(z)$ are the misidentification probabilities for pions and kaons, $\bar{f}^{\pi}_{uds}(z)$, $\bar{f}^{k}_{uds}(z)$ and $\bar{f}^{\mu}_{uds}(z)$ are the fractions of pions, kaons and decay'smuons (coming from π and K decays in flight) for uds flavour respectively, $\eta^{\mu}(z)$ is the muon identification efficiency for decay's muons, $\bar{f}^{o}_{uds}(z)$ and $\eta^{o}(z)$ are the fraction and the misidentification probability of *other* charged particles, which are mainly protons. The fractions for the different flavours and particles have been measured in DELPHI [19], and agree very well with the prediction obtained with the JETSET simulation program. The specific misidentification probabilities ($\eta^{\pi}(z)$, $\eta^{k}(z)$, ...) are supposed to be flavour independent, but since the fractions of particles are not the same in uds, c and b events, a different misidentification probability has to be evaluated for each flavour (η_{uds}, η_c and η_b). The equation (4) is used to extract $\eta^{\pi}(z)$, taking $\eta_{uds}(z)$ from the data and all the other quantities from the simulation. Then from the equations anologous to (4) written for c and b flavours, η_c and η_b are calculated.

The misidentification probalities obtained with this method have been compared with those obtained using a tight anti-b cut described in section 5.1 and a good agreement was observed (see reference [20] for more details).

Once the misidentification probability for each flavour has been computed, the number of fake muons per hemisphere for a variable z is obtained by multiplying them by the number of charged particles per hemisphere for each flavour. Subtracting these contaminations from the muon candidates per hemisphere, it is possible to estimate the distributions of genuine muons. Comparisons have been done in simulation between the distributions of genuine muons achieved by the subtraction with the true muon distributions directly taken from simulation, showing a good agreement.

8.3 Fitting of genuine muon distribution

In order to perform the measurement of the $BR(b \to \mu)$ and $BR(b \to c(\bar{c}) \to \mu)$, the following χ^2 function has been minimized:

$$\chi^2 = \sum_{i=1}^{m} \frac{\left(n_b^{g\mu}(z_i) - n_b^{g\mu,th}(z_i)\right)^2}{\sigma^2\left(n_b^{g\mu}(z_i)\right)} \tag{5}$$

where m is the number of bins, $n_b^{g\mu}(z_i)$ is the distribution of genuine muons measured in the previous section, and $n_b^{g\mu,th}(z_i)$ is a model expectation which can be written as:

$$\begin{aligned} n_b^{g\mu,th}(z) = N_{hem} R_b \left(1 + BR(g \to b\bar{b})\right) \\ \Big[\epsilon_{b\to\mu}^{glob}(z) P_{b\to\mu}(z) BR(b \to \mu) + \\ \epsilon_{b\to c(\bar{c})\to\mu}^{glob}(z) P_{b\to c(\bar{c})\to\mu}(z) BR(b \to c(\bar{c}) \to \mu)\Big] + \\ n_{b\to\tau\to\mu}^{\mu}(z) + n_{b\to J/\psi\to\mu}^{\mu}(z) + n_{g\to c\bar{c}\to\mu}^{\mu}(z) \end{aligned} \tag{6}$$

where $BR(b \to \mu)$ and $BR(b \to c(\bar{c}) \to \mu)$, are the only unknowns. $P_{b\to\mu}(z)$ and $P_{b\to c(\bar{c})\to\mu}(z)$ are the spectra of muons coming from $b \to \mu$ and $b \to c(\bar{c}) \to \mu$ decays. These spectra are taken from different models. For the central value, the ACCMM model for $b \to \mu$ decays and the ACCMM1 model for $c \to \mu$ decays have been used. $n_{b\to\tau\to\mu}^{\mu}(z)$, $n_{b\to J/\psi\to\mu}^{\mu}(z)$ and $n_{g\to c\bar{c}\to\mu}^{\mu}(z)$ are the contributions to *genuine* muons coming from $b \to \tau \to \mu$, $b \to J/\psi \to \mu$ and $g \to c\bar{c} \to \mu$ decays, respectively. The shape of these distributions have been taken directly from the simulation, but the recommendations of reference [10] have been followed for the normalization

The factors ϵ_k^{glob} are global efficiency factors which can be written as:

$$\epsilon_k^{glob}(z) = \epsilon_k^{cut}(z)\epsilon^{id}(z)\epsilon_k^{acc}(z) \tag{7}$$

where $\epsilon_k^{cut}(z)$ and $\epsilon_k^{acc}(z)$ are the efficiencies for the momentum cut ($p > 3\ GeV/c$) and the muon geometrical acceptance, for each of the considered channel k, respectively, and $\epsilon^{id}(z)$ is the muon identification efficiency.

Detailed tables with the results obtained for these correction factors are given in reference [20].

8.4 Results and systematic errors

The semileptonic branching ratios have been obtained by applying the binned χ^2 of equation (5) to the muon distributions of the previous section.

The first step is to apply the method to the simulated data. In these samples the generated values of the semileptonic branching ratios are known, so a comparison of the fit results with the generated ones can be performed. The difference between these values provides an information about the reliability of the method as well as corrections to be applied to the data. These differences take into account all the applied approximations.

The error on these correction factors have been taken from the statistical errors of the fits.

The next step is the application of the fitting procedure to the real data. The results obtained are shown in table 5. Some comments can be done about the statistical error

		$b \to \mu$ (%)	$b \to c(\bar{c}) \to \mu$ (%)	χ^2/dof
1992	P	10.56 ± 0.29	9.88 ± 0.54	$38.88/27$
	P_t^{in}	10.79 ± 0.26	9.60 ± 0.48	$35.19/32$
	P_t^{out}	10.74 ± 0.23	9.74 ± 0.42	$30.28/32$
1993	P	10.44 ± 0.29	9.54 ± 0.51	$36.22/27$
	P_t^{in}	10.52 ± 0.24	9.31 ± 0.45	$35.94/32$
	P_t^{out}	10.51 ± 0.23	9.26 ± 0.39	$43.68/32$
1994	P	10.83 ± 0.19	9.49 ± 0.35	$25.8/27$
	P_t^{in}	10.72 ± 0.17	9.48 ± 0.30	$35.5/32$
	P_t^{out}	10.59 ± 0.15	9.72 ± 0.27	$33.3/32$
1995	P	10.93 ± 0.29	9.55 ± 0.52	$25.0/27$
	P_t^{in}	10.71 ± 0.25	9.81 ± 0.46	$37.5/32$
	P_t^{out}	10.63 ± 0.22	9.94 ± 0.40	$40.5/32$

Table 5: Fit result for the real data (the errors are only statistical).

obtained. This error depends on the statistics of each year, but also on the fitting variable. The reason of this behavior can be found in the distribution of the different sources of *genuine* muons. Some variables are more discriminant than others, which separate the different contributions in different regions. For the transverse momentum, $b \to c(\bar{c}) \to \mu$ events are concentrated at low values, while $b \to \mu$ events are mainly situated in the high momentum region. On the other hand in the p distribution, in the low momentum region both contributions are of similar importance. Thus the errors on the semileptonic branching fractions extracted using the transverse momentum distributions are expected to be lower than those obtained using the momentum distributions.

Once the b semileptonic branching ratios have been fitted, it is possible to evaluate the $b \to \mu$ and the $b \to c(\bar{c}) \to \mu$ spectra using the model spectra $P_{b\to\mu}(z)$ and $P_{b\to c(\bar{c})\to\mu}(z)$. These spectra are displayed in figure 5 for each data taking year. The small contributions coming from the $b \to \tau \to \mu$ and $b \to J/\psi \to \mu$ decay channels, taken directly from the simulation, are also shown.

Sources of systematic uncertainties have been grouped into seven different categories. The first four categories are related to detector effects: muon identification and misidentification, hemisphere tagging, analysis method and Monte Carlo statistics. The other three take into account the theoretical knowledge on decays: fragmentation parameters, assumed branching ratios and decay models. In table 6 all these errors for $b \to \mu$ and $b \to c(\bar{c}) \to \mu$ as well as the range of variation are shown.

Averaging the three variables for each year, taking into account the correlations between the differents errors, the result obtained is:

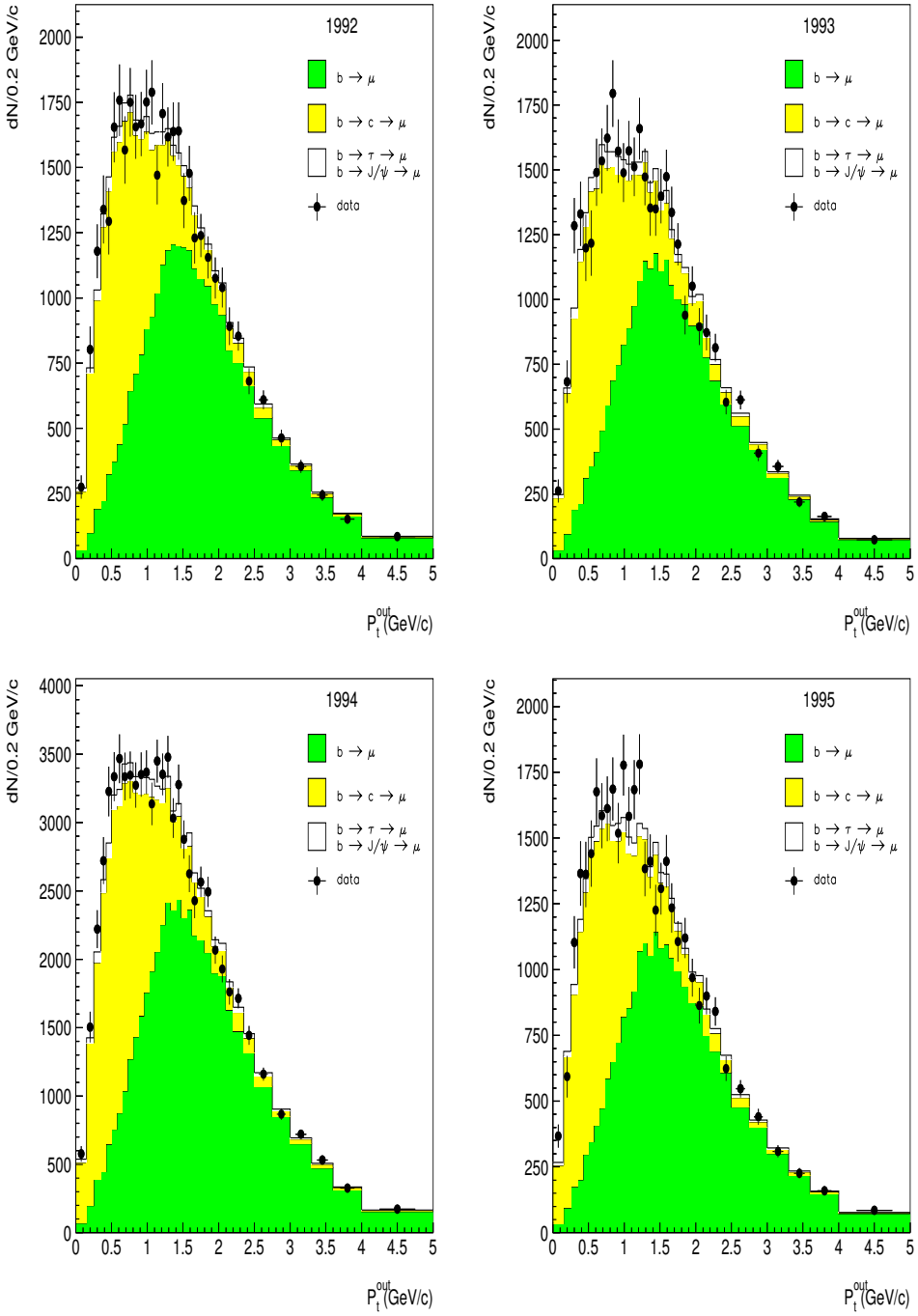

Figure 5: Comparison of the distributions of genuine muons for the b flavour in real data (dots) with the distributions obtained using the semileptonic branching ratios (histograms) with the variable p_t^{out}. The contributions of different processes are displayed.

Source	$\Delta(b \to \mu)$	$\Delta(b \to c(\bar{c}) \to \mu)$
Ef. id. barrel ($\pm 2.8\%$)	$\mp$ 0.190	$\mp$ 0.182
Ef. id. forward ($\pm 3.2\%$)	$\mp$ 0.022	$\mp$ 0.022
f^{π} ($\pm 2\sigma$)	$\mp$ 0.004	$\mp$ 0.008
$\bar{f}^{k}$ ($\pm 2\sigma$)	$\mp$ 0.002	$\mp$ 0.007
$\bar{f}^{\mu}$ ($\pm 2\sigma$)	$\pm$ 0.003	$\pm$ 0.009
$\bar{f}^{o}$ ($\pm 2\sigma$)	$\mp$ 0.001	$\mp$ 0.001
η^{π} ($\pm 2\sigma$)	$\mp$ 0.022	$\mp$ 0.120
$\alpha_{K\pi}$ ($\pm 2\sigma$)	$\pm$ 0.008	$\mp$ 0.035
η^{μ} ($\pm 2\sigma$)	$\mp$ 0.004	$\mp$ 0.004
η^{o} ($\pm 2\sigma$)	$\mp$ 0.001	$\mp$ 0.001
$\varepsilon^{uds}_{b-tight}$ ($\pm 15\%$)	$\pm$ 0.023	$\pm$ 0.010
$\varepsilon^{c}_{b-tight}$ ($\pm 15\%$)	$\pm$ 0.014	$\pm$ 0.055
Variable	$\pm$ 0.080	$\pm$ 0.150
Muon quality	$\pm$ 0.082	$\pm$ 0.082
Binning	$\pm$ 0.078	$\pm$ 0.079
MC statistics	$\pm$ 0.088	$\pm$ 0.163
$\langle X_E \rangle$ (0.702 ± 0.008)	$\pm$ 0.054	$\pm$ 0.099
$BR(b \to u)$ (2.6 ± 0.2)%	$\mp$ 0.008	$\mp$ 0.014
$BR(c \to \ell)$ (9.8 ± 0.5)%	$\mp$ 0.002	$\mp$ 0.003
$BR(b \to \tau \to \ell^-)$ (0.452 ± 0.074)%	$\mp$ 0.014	$\mp$ 0.096
$BR(b \to J/\psi \to \ell^-\ell^+)$ (0.07 ± 0.02) %	$\mp$ 0.036	$\mp$ 0.021
$BR(g \to b\bar{b})$ (0.269 ± 0.067) %	$\mp$ 0.033	$\mp$ 0.043
$BR(g \to c\bar{c})$ (2.33 ± 0.50)%	$\pm$ 0.009	$\pm$ 0.010
$b \to l$ $ACCMM^{+ISGW}_{-ISGW**}$	$^{-0.35}_{+0.43}$	$^{+0.52}_{-0.48}$
$c \to l$ $ACCMM1^{+ACCMM2}_{-ACCMM3}$	$^{-0.109}_{+0.105}$	$^{-0.124}_{+0.02}$

Table 6: Analysis III: Systematic uncertainties (%) for $BR(b \to l)$ and $BR(b \to c(\bar{c}) \to \mu)$

$$
\begin{aligned}
BR(b \to \mu) &= (10.64 \pm 0.11(stat) \pm 0.25(syst)^{-0.37}_{+0.44}(model))\% \\
BR(b \to c(\bar{c}) \to \mu) &= (9.59 \pm 0.20(stat) \pm 0.35(syst)^{+0.52}_{-0.49}(model))\%
\end{aligned}
$$

9 Analysis IV: Measurement of semileptonic b decays from inclusive B-reconstruction and charge correlation

In this analysis the charge correlation between the b quark and the lepton produced in its decay was used to measure the semileptonic decay rates of b-hadrons. The two different cases leading to the like charges, direct decay ($b \to \ell^-$) and "upper vertex" cascade decay ($b \to \bar{c} \to \ell^-$), were separated on the basis of different lepton momentum regions.

To use the charge correlation method effectively b-hadrons containing a b-quark, H_b, needed to be separated from those containing a $\bar{b}$-quark, $H_{\bar{b}}$. This separation was accomplished in four steps: by isolating b-quark events, by reconstructing the B decay vertex, by identifying the tracks from the B vertex and finally by estimating the hadron charge. The details of this method are described below and can be found in references [22, 23]. After the separation, the sign of the charge of the b-quark and that of the lepton were compared, and each lepton was classified into "like-sign" or "opposite-sign." In the fit of the like-sign spectrum, the direct decay $b \to \ell^-$ and cascade decay $b \to \bar{c} \to \ell^-$ were taken into account, whereas in the opposite-sign spectrum the cascade decay $b \to c \to \ell^+$ was taken into account.

9.1 B reconstruction and separation of H_b and $H_{\bar{b}}$

9.1.1 $b\bar{b}$ event tagging

Hadronic events were selected using the same requirements as in section 3. In addition the event thrust axis was required to be within the barrel region, $|\cos\theta_{thrust}| < 0.75$, to ensure a good b-tagging efficiency. These requirements led to 895662 and 397657 events in 1994 and 1995 data taking periods, respectively.

The combined b-tagging algorithm described in section 4 was used to select events containing b-hadrons with 66% efficiency and 91% purity.

9.1.2 Reconstruction of B vertex

In reconstructing the B decay vertex, the rapidity method presented in reference [21] was used. For the jet clustering algorithm, the transverse momentum cutoff was set at 5 GeV/c to prevent artificially dividing the large mass B jets into several jets. A raw B mass and energy were computed from the sum of the momentum vectors of the selected particles in the jet. These values were corrected depending on the reconstructed mass and hemisphere energy. This led to an energy resolution of about 7% for 75% of the b hadrons with the remainder being a non-gaussian tail at higher energies.

9.1.3 Identifying tracks from the B decay vertex

For each charged particle a probability, P_i, that the particle originated from a b-hadron decay rather than from fragmentation was calculated using an artificial neural network. It took into account the particle rapidity, momentum, its probability to originate from the primary vertex, its probability to originate from the fitted secondary vertex, the flight distance and the energy of the hemisphere. The top plot of figure 6 shows the comparison between the real data and the simulation.

9.1.4 Classification of H_b and $H_{\bar{b}}$

For each hemisphere, the vertex charge $Q_B = \sum Q_i P_i$ and its error $\sigma_{Q_B} = \sqrt{\sum P_i(1-P_i)}$ were calculated by using the probability, P_i, and the charge, Q_i, of each particle. These

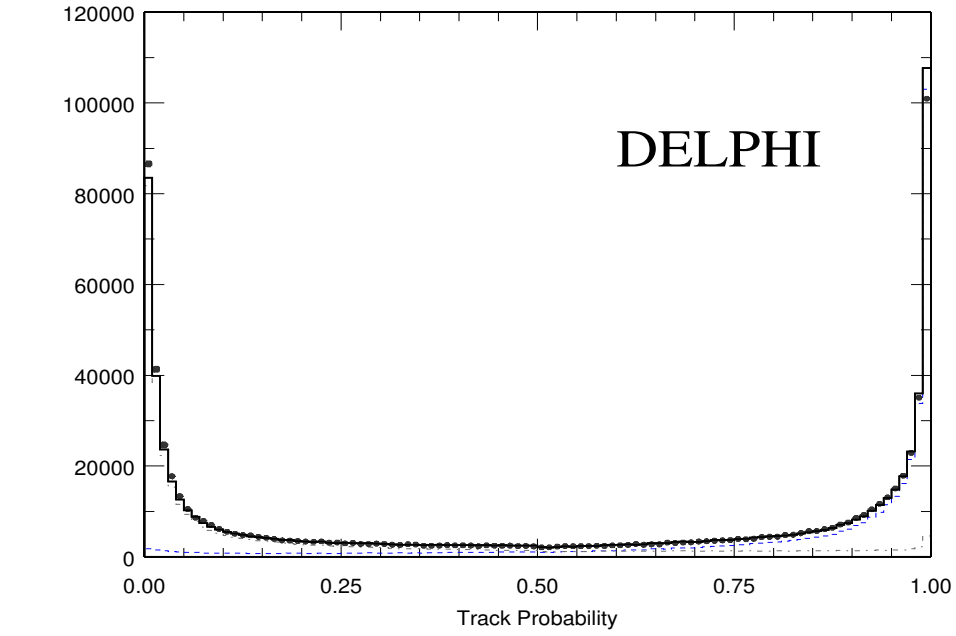

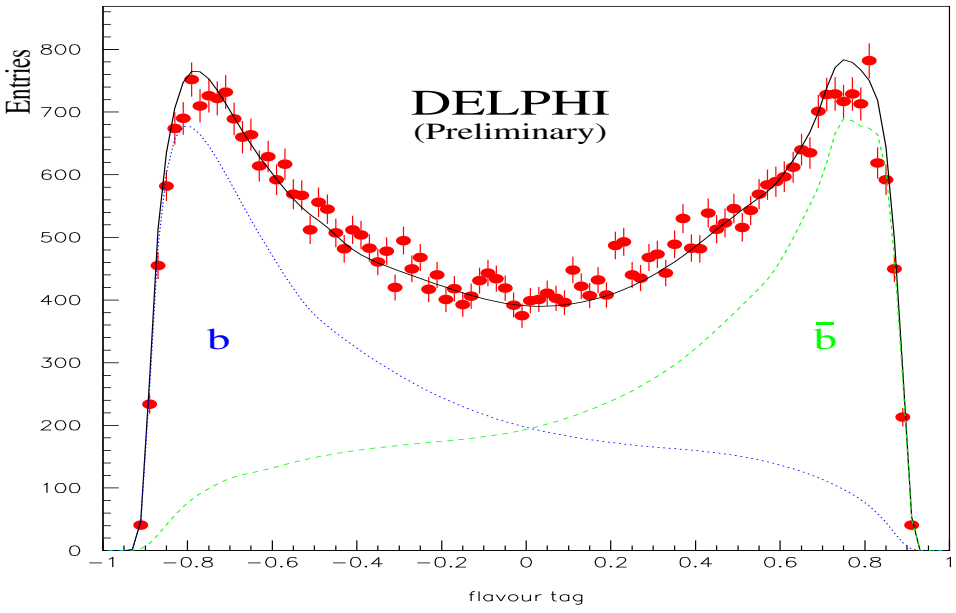

Figure 6: **Top**: Distribution of the track probability of real data compared to the simulation: Dotted (dashed) line represents the particles from fragmentation (from b-hadron decay). **Bottom**: Separation between H_b and $H_{\bar{b}}$ for real data compared to the simulation: dotted (dashed) line represents the H_b ($H_{\bar{b}}$) hemisphere.

values, combined with the charge of the identified kaon from b-hadron decay, the jet charge and the charge of the leading fragmentation particle were fed into a neural network to classify a b-hadron into H_b or $H_{\bar{b}}$. The bottom plot of figure 6 shows the comparison between the real data and the simulation.

9.2 Measurements

9.2.1 Lepton selection

The lepton identification was performed as in section 5. In addition, for each hemisphere, the lepton candidate was required to have come from the B decay vertex by requiring its probability P_i to be larger than 0.5.

For each selected lepton, its momentum k^* in the B rest frame was calculated using the B four-momentum from the secondary vertex fit and a rapidity constraint. Since the average resolution on k^* is 0.1 GeV/c, the k^* distribution was chosen with a bin width of $0.2GeV/c$ to reduce migration effects.

9.2.2 Fitting and results

The background contributions which may arise from non-b events, non-b-decay products and wrongly identified leptons were estimated from the simulation and subtracted. The differential decay rate for an identified lepton, $\frac{dN}{dk^*}(H_{\bar{b}} \to l^{\pm}X)$ was then calculated as:

$$\frac{dN}{dk^*}(H_{\bar{b}} \to l^{\pm}(k^*)X) = (N_i^{data} - N_i^{MC,bg}) \cdot \frac{N_i^{MC,gen}}{N_i^{MC,rec}} \frac{1}{k^*_{i+1} - k^*_i} \cdot \frac{1}{N(H_{\bar{b}})} \tag{8}$$

with bin definition $k^*_i < k^* < k^*_{i+1}$.

The background from the incorrectly determined charge of the b-quark was first estimated from the simulation and used in the fit. The results were then used to adjust the background level and branching fractions.

The following results have been obtained, and figure 7 shows the results of the fit using the ACCMM model:

	1994	1995	combined
BR($b \to \ell$)(%)	10.79 ± 0.14	10.86 ± 0.21	10.81 ± 0.12
BR($b \to \bar{c} \to \ell$)(%)	1.64 ± 0.24	1.32 ± 0.33	1.53 ± 0.20
BR($b \to c \to \ell$)(%)	7.98 ± 0.26	7.66 ± 0.38	7.87 ± 0.22

where the errors are only statistical.

9.3 Systematic errors

The following sources of systematic uncertainties have been considered:

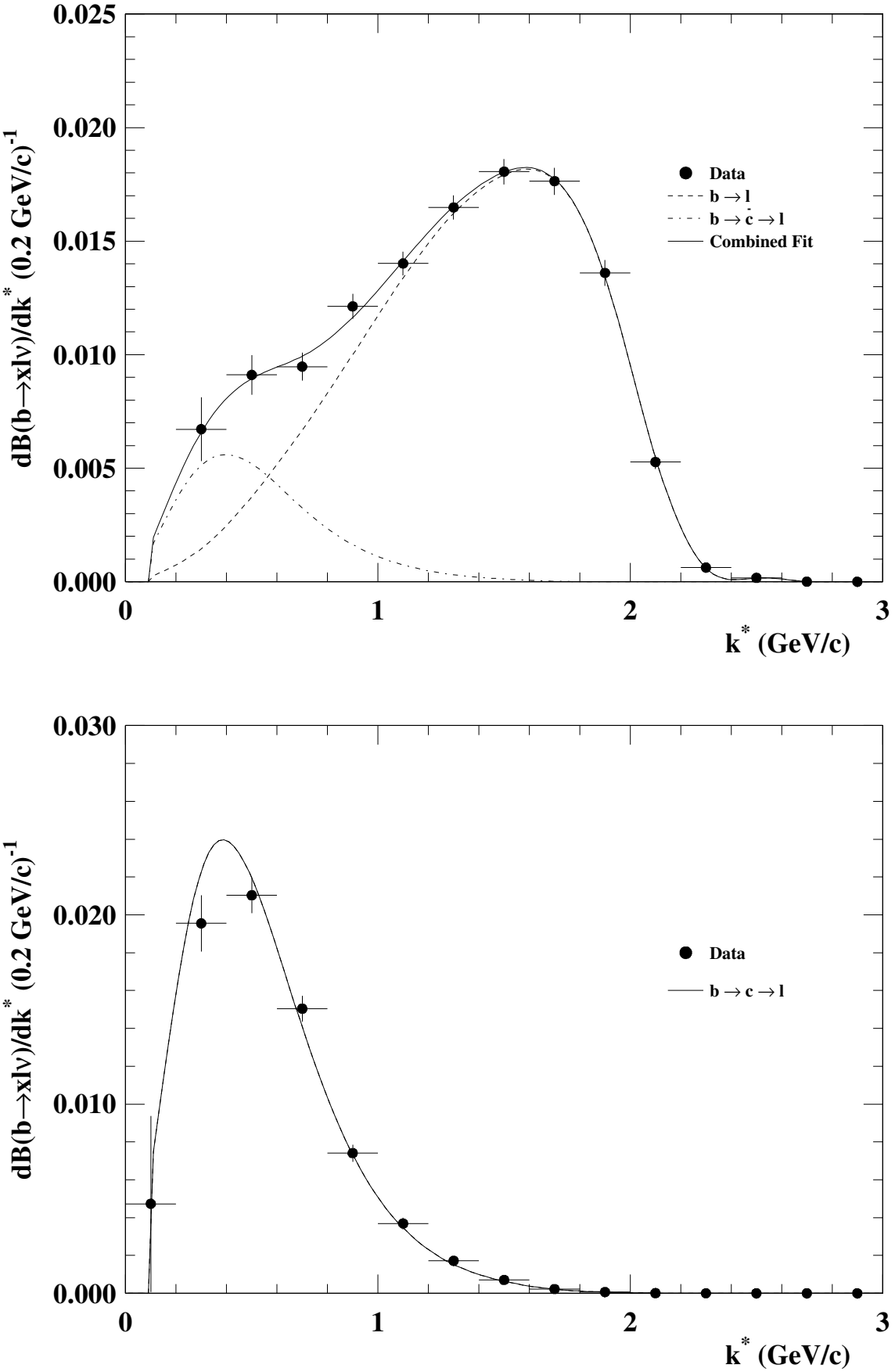

Figure 7: Lepton momentum spectra in the b-hadron rest frame. Top (bottom) plot shows the result of the fit with the ACCMM model to the like-sign (opposite-sign) sample .

- Track and lepton selection:
  The muon and electron identification efficiencies and the background due to hadron misidentification were varied considering their measurement errors in the data-simulation comparisons (see sections 5.1,5.2) as in Analysis I. The residual contamination in the electron sample due to converted photons has been varied by $\pm$ 10%.

  The probability for a particle to be a b-hadron decay product has been varied by $\pm$ 10 %.

- b-tagging
  The b-tagging method, described in 4, selected events where a secondary vertex had been successfully reconstructed. This requirement introduced a bias in the composition of the selected b-hadron sample. In addition, requiring a B vertex reconstruction and the b-charge determination introduced an additional bias. In order to study the effect of the bias, the compositions in b-hadrons of simulated events before and after imposing these requirements were compared. The b-hadrons with longer lifetimes were favoured as a result of such requirements. The results were then used to reweight the simulation, and a variation of one standard deviation of the statistics was used as uncertainty.

  The stability of the results as a function of the cut on the b-tagging variable was checked and the effect of a variation of $\pm$ 5% was considered as systematic error.

- Fitting
  The error due to the finite Monte Carlo statistics in the fitting procedure was evaluated.

  When performing simultaneous fits of both like-sign and opposite-sign histograms, a degree of convergence between both sides was manually set. The degree of convergence to insure stable results has been varied by 10%.

  The resolution on the k^* variable was varied by $\pm$20% to account for the uncertainty in the B reconstructed energy and for binning effects.

- B reconstruction
  The output of the neural net, used to determine the charge of decaying b-hadrons, was studied by varying its efficiency by $\pm$10%.

- Models
  Effects due to the b quark fragmentation function have been studied by varying the ϵ_b parameter in the Peterson fragmentation function [13].

  The lepton distribution from the "upper vertex" was studied by varying the contributions of $D_s \to \ell^- X$ and $\bar{D}^0(D^-) \to \ell^- X$ as suggested in reference [10].

  The modelling uncertainty related to the branching ratios assumed for $b \to \tau \to \ell$, $b \to J/\Psi \to \ell$ and to different lepton decay models was also calculated according to [10].

Source	Range	ΔBR $(b \to \ell)$ x10^{-2}	ΔBR $(b \to \bar{c} \to \ell)$ x10^{-2}	ΔBR $(b \to c \to \ell)$ x10^{-2}
ϵ_e	$\pm 3\%$	∓ 0.18	∓ 0.05	∓ 0.15
ϵ_μ	$\pm 2.8\%$	∓ 0.14	∓ 0.03	∓ 0.11
Misidentified e	$\pm 8\%$	± 0.01	∓ 0.10	∓ 0.08
Misidentified μ	$\pm 6.5\%$	± 0.01	∓ 0.09	∓ 0.05
Converted γ	$\pm 10\%$	± 0.01	∓ 0.04	∓ 0.03
P_b	$\pm 10\%$	± 0.01	∓ 0.04	∓ 0.06
b-hadron species	$\pm 5\%$	∓ 0.04	∓ 0.02	∓ 0.03
b-tagging	$\pm 5\%$	± 0.02	± 0.02	± 0.10
b-charge resolution	$\pm 10\%$	± 0.01	± 0.07	∓ 0.10
MC statistics		∓ 0.02	∓ 0.04	∓ 0.09
Fitting	$\pm 10\%$	< 0.01	± 0.01	∓ 0.01
k^* resolution	$\pm 20\%$	± 0.02	∓ 0.07	± 0.05
B fragmentation	$\pm 20\%$	∓ 0.06	∓ 0.03	∓ 0.06
$\frac{b\to W\to D}{b\to W\to D_s}$	$(1.28^{+1.52}_{-0.61})$	$^{+0.04}_{-0.06}$	$^{-0.09}_{+0.08}$	$^{+0.03}_{-0.03}$
$Br(b \to \tau \to \ell)$	$(0.452 \pm 0.074)\%$	∓ 0.04	∓ 0.04	< 0.01
$Br(b \to J/\Psi \to \ell)$	$(0.07 \pm 0.02)\%$	∓ 0.07	± 0.03	∓ 0.02
$Br(c \to \ell)$	$(9.8 \pm 0.5)\%$	∓ 0.03	∓ 0.13	∓ 0.05
Total systematic		± 0.26	± 0.26	± 0.30
Decay models				
$b \to \ell$ model	ACCMM $(^{+ISGW}_{-ISGW**})$	$^{-0.35}_{+0.52}$	$^{+0.30}_{-0.41}$	$^{+0.04}_{-0.04}$
$c \to \ell$ model	ACCMM1 $(^{+ACCMM2}_{-ACCMM3})$	$^{-0.05}_{+0.05}$	$^{+0.03}_{-0.03}$	$^{-0.21}_{+0.10}$
Total Models		$^{-0.35}_{+0.52}$	$^{+0.30}_{-0.41}$	$^{-0.21}_{+0.11}$

Table 7: Analysis IV: Summary of systematic uncertainties

The summary concerning the different contributions to systematic uncertainties is given in Table 7.

In conclusion, with the method of charge correlation, the following results have been obtained from the data collected with the DELPHI detector in 1994 and 1995:

$$\begin{aligned} BR(b \to \ell) &= (10.81 \pm 0.12(stat) \pm 0.26(syst)^{-0.35}_{+0.52}(model))\% \\ BR(b \to \bar{c} \to \ell) &= (1.53 \pm 0.20(stat) \pm 0.26(syst)^{+0.30}_{-0.41}(model))\% \\ BR(b \to c \to \ell) &= (7.87 \pm 0.22(stat) \pm 0.30(syst)^{-0.21}_{+0.11}(model))\% \end{aligned}$$

10 Combinations of results

Several different analyses have been performed, as described in previous sections, and a comparison of all results is shown in Table 8.

A procedure to combine them in order to produce a final set of physical parameters has been developed. The basic technique is the one named BLUE [24], which determines the

	An.I	An. II	An. III	An. IV
BR(b$\to\ell^-$)%	$\mathbf{10.66 \pm 0.11 \pm 0.24^{-0.25}_{+0.42}}$	$\mathbf{10.68 \pm 0.14 \pm 0.31^{-0.31}_{+0.50}}$	$\mathbf{10.64 \pm 0.11 \pm 0.25^{-0.37}_{+0.44}}$	$\mathbf{10.81 \pm 0.12 \pm 0.26^{-0.35}_{+0.52}}$
BR(b$\to$c$\to\ell^+$)%	$\mathbf{8.08 \pm 0.37 \pm 0.38^{-0.31}_{+0.23}}$	$\mathbf{7.22 \pm 0.66 \pm 0.35^{-0.31}_{+0.45}}$		$\mathbf{7.87 \pm 0.22 \pm 0.30^{-0.21}_{+0.11}}$
BR(b$\to\bar{\text{c}}\to\ell^-$)%	$\mathbf{1.68 \pm 0.33 \pm 0.25^{-0.23}_{+0.14}}$	$\mathbf{2.00 \pm 0.45 \pm 0.38^{-0.74}_{+0.50}}$		$\mathbf{1.53 \pm 0.20 \pm 0.26^{-0.41}_{+0.30}}$
BR(b$\to$c$\to\ell^+$)+	9.76$\pm$0.23$\pm$0.43	9.22$\pm$0.71$\pm$0.48	$\mathbf{9.59 \pm 0.20 \pm 0.35^{-0.49}_{+0.52}}$	9.40$\pm$0.26$\pm$0.34
BR(b$\to\bar{\text{c}}\to\ell^-$)%				

Table 8: Comparison of the results of the different analyses. Boldface values are used for the measurements, slimface values are sums which are only shown for comparison.

best estimate of a physical quantity built by a linear combination of the results obtained by several experiments. The estimate is then given by the following quantity:

$$\hat{y} = \sum \alpha_i y_i \tag{9}$$

where the coefficients α_i are built from the covariance matrix E_{ij} of the measured parameters. The method may be easily applied to determine several physical parameters simultaneously, by replacing that matrix with the more general one $\mathsf{E}_{i\alpha j\beta}$ where the indices i, j refer to the measurements and α, β identify the parameters.

In order to apply this technique, it is necessary to estimate the off-diagonal elements of the full error matrix E . Thus the statistical error $\sigma_{i\alpha}$ of each parameter α determined by the analysis i has been splitted into two terms: the first one is computed from the observed number of leptons and is considered as fully correlated with the corresponding errors from other measurements; the other is computed in order to keep the same total error and is assumed as being uncorrelated.

The estimation of the correlation between the parameters of different analyses is a bit more complicated, as it is necessary to account for the correlation already present inside each single analysis. A reasonable criterion for that is to build the covariance elements by multiplying the two correlated terms of $\sigma_{i\alpha}$, described above, and by applying a correlation factor determined as an average of the coefficients resulting from the different analyses.

As the different analyses are used with somewhat different data samples, while the described procedure can be applied only for identical samples, the full statistic has been divided into non-overlapping subsamples, assuming for each sample an error which scales with the square root of the number of events. As the multivariate analysis builds up the genuine muon distributions by a linear combination of distributions obtained in 6 categories, the overlap with the b-tagged sample used by the other analyses has been conservatively assumed as corresponding to the category with the largest coefficient α_i .

The results are listed in table 9.

			$\pm stat.$	$\pm exp.syst.$	$\pm phys.syst.$	$\begin{matrix} IGSW \\ IGSW** \end{matrix}$	$\begin{matrix} ACCMM2 \\ ACCMM3 \end{matrix}$
BR(b$\to\ell^-$)	=	0.1065	$\pm$0.0007	$\pm$0.0024	$\pm$0.0006	$\begin{matrix} -0.0027 \\ +0.0041 \end{matrix}$	$\begin{matrix} -0.0009 \\ +0.0008 \end{matrix}$
BR(b$\to$c$\to\ell^+$)	=	0.0788	$\pm$0.0013	$\pm$0.0026	$\pm$0.0007	$\begin{matrix} +0.0031 \\ -0.0034 \end{matrix}$	$\begin{matrix} -0.0016 \\ +0.0006 \end{matrix}$
BR(b$\to\bar{\text{c}}\to\ell^-$)	=	0.0171	$\pm$0.0013	$\pm$0.0033	$\pm$0.0015	$\begin{matrix} +0.0018 \\ -0.0024 \end{matrix}$	$\begin{matrix} +0.0001 \\ -0.0002 \end{matrix}$
$\bar{\chi}_b$	=	0.127	$\pm$0.013	$\pm$0.006	$\pm$0.002	$\begin{matrix} -0.003 \\ +0.004 \end{matrix}$	$\begin{matrix} -0.003 \\ +0.003 \end{matrix}$

Table 9: Combined results of the measured quantities; the systematic error quoted as *phys.syst.* includes the uncertainties arising from input physical parameters as branching ratios and gluon splitting rates

To investigate the effect of the main assumptions done in this analysis (estimation of the correlated part of the error, estimation of the correlation coefficient between different parameters determined in different analyses) the procedure has been repeated after

	$BR(b\to\ell^-)$	$BR(b\to c\to\ell^+)$	$BR(b\to\bar{c}\to\ell^-)$	$\bar{\chi}_b$
$BR(b\to\ell^-)$	1.00	-0.396	-0.031	.038
$BR(b\to c\to\ell^+)$	0.625	1.00	-0.475	-0.034
$BR(b\to\bar{c}\to\ell^-)$	0.112	-0.095	1.00	0.015
$\bar{\chi}_b$	0.018	-0.083	-0.052	1.00

Table 10: Correlation matrix of combined results. On the upper-right side the statistical coefficients are reported, on the lower-left side the statistical+experimental systematic coefficents are shown

changing them slightly. The off-diagonal element in the error matrix has been changed with the smallest of the two corresponding diagonal elements, different estimations of the correlation coefficient between different parameters in different analyses have also been tried. Compatible results have been obtained.

11 Conclusions

Four different analyses have been used to measure the semileptonic branching ratios for primary and cascade b decays in hadronic Z decays. Results are compatible and a global average has been obtained:

$$\begin{aligned}
BR(b\to\ell^-) &= (10.65 \pm 0.07(stat) \pm 0.25(syst)^{-0.28}_{+0.42}(model))\% \\
BR(b\to c\to\ell^+) &= (7.88 \pm 0.13(stat) \pm 0.27(syst)^{-0.38}_{+0.32}(model))\% \\
BR(b\to\bar{c}\to\ell^-) &= (1.71 \pm 0.13(stat) \pm 0.36(syst)^{-0.25}_{+0.19}(model))\% \\
\bar{\chi}_b &= 0.127 \pm 0.013(stat) \pm 0.007(syst) \pm 0.005(model)
\end{aligned}$$

Error Source	Range	ΔBR(b$\to\ell^-$) 10^{-2}	ΔBR(b$\to$c$\to\ell^+$) 10^{-2}	ΔBR(b$\to\bar{\text{c}}\to\ell^-$) 10^{-2}	$\Delta\bar{\chi}_b$ 10^{-2}
$\langle x_E(\text{c})\rangle$	0.484 ± 0.008	∓ 0.01	<0.01	∓ 0.01	± 0.06
$\frac{b\to W\to D}{b\to W\to D_s}$	$(1.28^{+1.52}_{-0.61})$	± 0.02	± 0.03	∓ 0.08	∓ 0.01
Br(b $\to \tau \to \ell$)	$(0.452 \pm 0.074)\%$	∓ 0.02	∓ 0.05	∓ 0.02	<0.01
Br(b $\to$ J/$\psi \to \ell^+\ell^-$)	$(0.07 \pm 0.02)\%$	∓ 0.05	± 0.01	<0.01	∓ 0.23
Br(c $\to \ell$)	$(9.8 \pm 0.5)\%$	∓ 0.01	∓ 0.01	∓ 0.12	∓ 0.01
g $\to$ c$\bar{\text{c}}$	$(2.33 \pm 0.50)\%$	± 0.01	± 0.01	∓ 0.01	<0.01
g $\to$ b$\bar{\text{b}}$	$(0.269 \pm 0.067)\%$	∓ 0.02	∓ 0.03	± 0.03	± 0.01

Table 11: Breakdown of physics systematic uncertainties in the combined values

References

[1] DELPHI Collaboration, P. Aarnio et al., Nucl. Inst. Meth. **A303** (1991) 233;
DELPHI Collaboration, P. Abreu et al., Nucl. Inst. Meth. **A378** (1996) 57

[2] N. Bingefors et al., Nucl. Inst. Meth. **A328** (1993) 447.
V. Chabaud et al., Nucl. Inst. Meth. **A368** (1996) 314.

[3] T. Sjöstrand CERN-TH/7112/93 (1993), revised August 1995; Comp. Phys. Comm. **82** (1994) 74.

[4] JADE Collaboration, W.Bartel et al., Z. Phys. **C33** (1983) 23; S.Bethke et al., Phys. Lett. **B213** (1988) 235.

[5] DELPHI Collaboration, P. Abreu et al.,
A precise measurement of the partial decay width ratio $R_b^0 = \Gamma_{b\bar{b}}/\Gamma_{had}$
CERN-EP/98-180 Submitted to E.Phys.J.

[6] G.R.Wilkinson *Improvements to the Muon Identification in the 94C2 Short DST Production*
DELPHI note 97-37 PHYS 690

[7] C.Kreuter *Electron Identification using a Neural Network*
DELPHI note 96-169 PHYS 658

[8] M. Bauer et al., Z. Phys. **C34** (1987) 103.

[9] Particle Data Group Eur Phys. J. **C3** (1998) 1.

[10] The LEP Electroweak Working Group
Input Parameters for the LEP/SLD Electroweak Heavy FlavorResults LEPHF/98-01, July, 1998 Geneva
http://www.cern.ch/LEPEWWG/heavy/

[11] DELPHI Collaboration, P. Abreu et al., Z. Phys. **C66** (1995) 323

[12] The LEP Collaborations ALEP, DELPHI, L3, OPAL, the LEP Electroweak Working Group and the SLD Heavy Flavour Group
A Combination of Preliminary Electroweak Measurements and Constraints on the Standard Model
CERN-EP/99-15, 8 FEB 1999.

[13] C.Peterson et al., Phys.Rev. **D27** (1983) 105.

[14] DELPHI Collaboration, P. Abreu et al., Z.Phys.**C 74** (1997) 19.

[15] DELPHI Collaboration, P. Abreu et al., Z.Phys.**C 71** (1996) 539.

[16] DELPHI Collaboration, P. Abreu et al.,
"Search for $B_s - \bar{B}_s$ mixing, measurement of the B_s lifetime and of $\Delta\Gamma/\Gamma$ - an update"
DELPHI internal note 99-109 CONF 296
contributed paper number 4-520 to this conference

[17] P. Billoir et al., Nucl. Inst. Meth. **A360** (1995) 532.

[18] Ch. de la Vaissière and F. Martínez-Vidal *Description and performances of the DELPHI multivariate flavour tagging* DELPHI 97-134 PHYS 721.

[19] DELPHI Collaboration, P. Abreu et al.,
E. Phys. J. **C5**(1998) 585.

[20] E. Cortina et al., *Measurement of the b Semileptonic Branching Ratios by applying Multitag Techniques*, DELPHI 99-3 PHYS 815.

[21] DELPHI Collaboration, P. Abreu et al.,
Z. Phys. C 68 (1995) 353

[22] Z. Albrecht et al., *BSAURUS - inclusive B-reconstruction for DELPHI data*, http://home.cern.ch/ pubxx/tasks/bcteam/www/inclusive/bsaurus.html

[23] M. Feindt et al., *Measurement of inclusive branching ratios of the B^+ meson*, DELPHI 97-100 CONF 82, contribution to HEP'97 Conference, Jerusalem 1997..

[24] L. Lyons et al., Nucl. Inst. Meth. **A270** (1988) 110-117.